Earth, Planets and Space

FULL PAPER Open Access

Preparation zones for large crustal earthquakes consequent on fault-valve action

Richard H. Sibson[1,2*]

Abstract

A combination of geological evidence (in the form of hydrothermal vein systems in exhumed fault systems) and geophysical information around active faults supports the localized invasion of near-lithostatically overpressured aqueous fluids into lower portions of the crustal seismogenic zone which commonly extends to depths between 10 and 20 km. This is especially the case for compressional–transpressional tectonic regimes which, beside leading to crustal thickening and dewatering through prograde metamorphism, are also better at containing overpressure and are 'load-strengthening' (mean stress rising with increasing shear stress), the most extreme examples being associated with areas undergoing active compressional inversion where existing faults are poorly oriented for reactivation. In these circumstances, 'fault-valve' action from ascending overpressured fluids is likely to be widespread with fault failure *dual-driven* by a combination of rising fluid pressure in the lower seismogenic zone lowering fault frictional strength, as well as rising shear stress. Localized fluid overpressuring nucleates ruptures at particular sites, but ruptures on large existing faults may extend well beyond the regions of intense overpressure. Postfailure, enhanced fracture along fault rupture zones promotes fluid discharge through the aftershock period, increasing fault frictional strength before hydrothermal sealing occurs and overpressures begin to reaccumulate. The association of rupture nucleation sites with local concentrations of fluid overpressure is consistent with selective invasion of overpressured fluid into the roots of major fault zones and with observed non-uniform spacing of major hydrothermal vein systems along exhumed brittle–ductile shear zones. A range of seismological observations in compressional–transpressional settings are compatible with this hypothesis. There is a tendency for large crustal earthquakes to be associated with extensive ($L \sim 100$–200 km) low-velocity zones in the lower seismogenic crust, with more local *Vp/Vs* anomalies ($L \sim 10$–30 km) associated with rupture nucleation sites. In some instances, these low-velocity zones also exhibit high electrical conductivity. Systematic, rigorous evaluation is needed to test how widespread these associations are in different tectonic settings, and to see whether they exhibit time-dependent behaviour before and after major earthquake ruptures.

Keywords: Compressional–transpressional faulting, Fluid overpressures, Gold transport, Lower seismogenic zone, Dual-driven failure, Fault-valve action, Low-velocity zones, *Vp/Vs* anomalies

Introduction

In deforming quartzo-feldspathic crust away from areas of active subduction, seismic activity is largely restricted to the top 15 ± 5 km of the crust with the base of this seismogenic zone (b.s.z.) apparently bounded by isotherms defining the onset of crystal plasticity in quartz (c. 350 °C) and plagioclase feldspar (c. 450 °C) (Sibson 1984; Ito 1999). Anderson (1905) argued that Earth's free surface, incapable of sustaining shear stress, imposes an important mechanical boundary condition requiring one of the principal compressive stresses ($\sigma_1 > \sigma_2 > \sigma_3$) to be vertical and the other two to lie in a horizontal plane. While topography may impose short wavelength stress heterogeneity in the near-surface, this diminishes with depth so that formation or reactivation of faults and fractures generally occurs under three basic stress regimes where

*Correspondence: rick.sibson@otago.ac.nz
[1] Department of Geology, University of Otago, P.O. Box 56, Dunedin 9054, New Zealand
Full list of author information is available at the end of the article

σ_v=σ_1 (normal fault regime), σ_v=σ_2 (wrench or strike–slip fault regime), or σ_v=σ_3 (thrust fault regime). A range of evidence supports the predominance of 'Andersonian' stress trajectories through much of the Earth's seismogenic crust (e.g. Célérier 2008; Zoback 1992), and it will generally be assumed that 'Andersonian' horizontal or vertical stress trajectories prevail in the discussion that follows on fault formation and reactivation. Further justification comes from a global dip histogram for near-pure reverse-slip ruptures showing a dip range, $0<\delta<60°$, with a dominant peak at $\delta=30°$ and truncation at $\delta=60°$ (Sibson 2012), both consistent with optimal reactivation and frictional lock-up on the assumption of horizontal σ_1, for a friction coefficient, $\mu_s=0.6$ (close to the bottom of Byerlee's (1978) range for hard-rock friction).

Where pore and fracture space is pervaded by fluid, all normal stresses are reduced by the pore-fluid pressure, P_f, so that the triaxial stress state is represented by effective principal compressive stresses $(\sigma_1' = (\sigma_1 - P_f) > \sigma_2' = (\sigma_2 - P_f) > \sigma_3' = (\sigma_3 - P_f))$ (Hubbert and Rubey 1959). Taking account of effective stress, the condition for reshear overcoming the frictional shear strength of the fault, τ_f, is then approximated by a criterion of Coulomb form:

$$\tau = \tau_f = C_f + \mu_s(\sigma_n - P_f) \quad (1)$$

where τ and σ_n are, respectively, the components of shear and normal stress acting on the fault, μ_s is the static coefficient of friction (here assumed to be time-independent), and C_f is the fault cohesive strength which may itself be time-varying. Commonly, it is supposed that the principal driver to failure is increasing differential stress, $(\sigma_1-\sigma_3)$, raising shear stress, τ, on the fault. However, in nature it is generally not possible to change shear stress on a fault without also increasing or decreasing σ_n in some manner (Sibson 1993).

Reshear can also be induced by increasing P_f which lowers the effective normal stress clamping fault walls together (Raleigh et al. 1976). Heightened appreciation of this failure mechanism comes from increased recognition of earthquakes induced by fluid injection down boreholes in recent years (e.g. Nicholson and Wesson 1990; Ellsworth 2013; Grigoli et al. 2018). This raises important questions as to whether natural fault failure in the Earth may, in some circumstances, be *'dual-driven'* involving increases in pore-fluid pressure as well as shear stress, and whether fluid pressure cycling is widespread in seismogenic crust (Sibson 2020). Hacker (1997) and Ague et al. (1998) have suggested, for instance, that metamorphic dehydration reactions in the mid-crust may contribute to brittle failure through generation of fluid overpressure.

In the general context of fault reactivation mechanics this paper reviews geological and geophysical observations supporting the existence of dual-driven seismogenic fault failure in fluid-overpressured crust. Rupturing through overpressured crust may lead to fluid discharge along faults postfailure (fault-valve activity), affecting their strength. Evidence for such activity varies with tectonic setting but is strongest in compressional–transpressional regimes where there is potential for the development of recognizable preparation zones prior to large earthquakes.

Fluid pressure regimes

Pore-fluid pressure at a depth, z, in the crust is usefully related to the vertical stress or overburden pressure, σ_v=ρgz (where ρ is the average rock density and g the gravitational acceleration), by the pore-fluid factor:

$$\lambda_v = P_f / \sigma_v \quad (2)$$

(Hubbert and Rubey 1959), where aqueous fluid occupying pores and/or fractures is interconnected through to the earth's surface the fluid-pressure is hydrostatic ($\lambda_v \sim 0.4$), assuming water and rock densities of *c.* 1000 and 2650 kg/m^3, respectively (Fig. 1). This is equivalent to the pressure at the bottom of a well to the same depth. In many compacting or deforming sedimentary basins, pore-fluids are overpressured above hydrostatic ($\lambda_v > 0.4$), in some instances achieving near-lithostatic conditions ($\lambda_v \rightarrow 1.0$) (e.g. Yerkes et al. 1990; MacPherson and Garven 1999; Osborne and Swarbrick 1997) (Fig. 1). However, on the evidence of vein assemblages, fluid overpressures may also develop in crystalline crust. For instance, the presence of flat-lying extension veins (Figs. 2 and 8) demonstrates that overpressures in compressional stress regimes (where σ_v=σ_3) sometimes exceed the lithostatic load (e.g. Foxford et al. 2000; Tunks et al. 2004; Japas et al. 2016). Commonly, these flat-lying vein systems occur in proximity to mid-crustal shear zones defining steep reverse fault structures (e.g. Sibson et al. 1988; Robert et al. 1995; Miller and Wilson 2004) which act as fluid conduits with impermeable hydrothermal 'chokes' (Henderson and McCaig 1996) but some also develop in association with granitoid cupolas.

Overpressures in seismogenic crust

An important question is the extent to which pore-fluids overpressured above hydrostatic are present in seismogenic crust. It has been argued (e.g. Townend and Zoback 2000) that distributed seismic activity within crystalline upper crust renders it too permeable for overpressures to accumulate and be sustained. If such is the case, hydrostatic fluid-pressures would prevail throughout

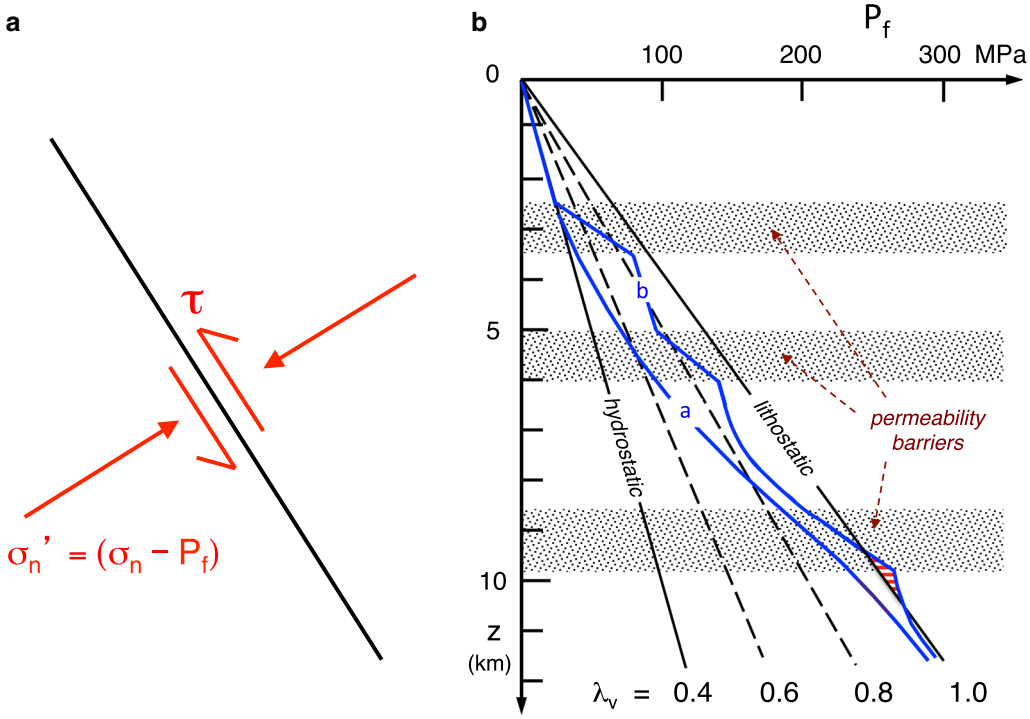

Fig. 1 **a** Components of shear stress, τ, and normal stress, σ_n, acting on a fault; **b** hypothetical profiles of pore-fluid pressure, P_f, versus depth, z, within the crust and in crustal fault zones shown in relation to the pore-fluid factor, λ_v. Profile a assumes a smooth progression from hydrostatic towards lithostatic pressure as permeability steadily reduces with increasing depth; profile b is affected by the presence of low-permeability barriers (area of cross-hatching notes region of supralithostatic pore pressure). Note that the fluid-pressure profile inside a fault zone may differ from that in the wallrock

Fig. 2 Swarm of predominantly subhorizontal quartz-infilled extension veins disrupting Calaveras slates, near Carson Hill, Mother Lode belt, CA (David P. Hill for scale)

the entire seismogenic crust. However, deeper portions of the seismogenic zone ($T > c.$ 200 °C) are active hydrothermal environments (e.g. Huston 1998) where dissolution and precipitation of silica and other solutes may be widespread, clogging pore and fracture space. Indications form experiments on gouge compaction under hydrothermal conditions comparable to the lower seismogenic zone are that permeability may be reduced by orders of magnitude over time periods that are short compared with the recurrence intervals for large earthquakes (e.g. Morrow et al. 2001; Silvio et al. 2007). Moreover, the tectonic stress field plays an important role in controlling the maximum overpressure that can be sustained without activating faults and fractures that would allow drainage (Sibson 2003). Evidence is also accumulating from fluid inclusion analyses in crystalline basement assemblages of fluid-pressure cycling between near-lithostatic and near–hydrostatic levels of pore-fluid pressure, attributable to 'fault-valve' discharge from overpressured portions of the crust (e.g. Marchesini et al. 2019).

Compressional stress fields with $\sigma_v = \sigma_3$ allow for the greatest overpressures to be sustained without fault/fracture activation. Thus, it is difficult to believe that thrust ruptures such as those responsible for the 1983 **M**6.3 Coalinga and 1985 **M**6.1 Kettleman Hills earthquakes occurring at *c.* 10 km depth below overpressured sedimentary sequences in association with pronounced low-velocity zones (Eberhart-Phillips 1989; Yerkes et al. 1990) were not nucleating in fluid-overpressured crust. While the case for rupturing in fluid-overpressured crust

is most compelling for thrust and steep reverse faulting events (Sibson 2014), overpressures have also been inferred from geophysical observations for other faulting modes, most commonly towards the base of the seismogenic upper crust over temperatures between perhaps 250° and 350 °C, corresponding broadly with the prehnite–pumpellyite facies metamorphic environment where geological evidence for local overpressuring is widespread (e.g. De Ronde et al. 2001).

Geological signatures of fluid overpressure

Macroscopic extension veins often infilled with fibrous minerals recording crack-seal growth (Ramsay 1980) are recognized as the product of hydraulic extension fracturing, forming perpendicular to σ_3 when:

$$P_f > \sigma_3 + T_o \quad (3)$$

under conditions of low differential stress $(\sigma_1 - \sigma_3) < 4T_o$ (Secor 1965; Etheridge 1983). Longitudinal dimensions of such veins commonly range from centimetres to metres, but in extreme cases range up to a kilometre or more (e.g. Foxford et al. 2000). Systematic arrays of extension veins (see Fig. 8) thus demonstrate local attainment of the *tensile overpressure condition* ($P_f > \sigma_3$) at some time in the history of the rock mass (Sibson 2017). Where such extension veins are flat-lying (e.g. Figs. 2 and 8a) they provide evidence of supralithostatic fluid overpressures unless remarkable stress heterogeneity existed at the time of their formation. Material heterogeneity may affect the mode of brittle failure so that sets of parallel extension veins may evolve into distributed fault–fracture meshes made up of interlinked shear and extensional fractures (Sibson 1996).

Combining the hydraulic fracture criterion (Eq. 3) with the limiting differential stress proviso for the three basic stress regimes with $\sigma_v = \sigma_1$, σ_2, or σ_3 (Secor 1965) makes it possible to construct plots of λ_v versus depth, defining the pore-fluid pressure condition needed to form hydraulic extension fractures at different depths (Fig. 3). While vertical extension veins may form at shallow depth (less than a kilometre or so) in normal fault (and, to a lesser extent, in strike–slip) stress regimes under hydrostatic fluid pressure, vein formation at greater depth requires suprahydrostatic fluid-pressures. In compressional thrust-fault regimes, supralithostatic fluid-pressures are required at all depths for the formation of subhorizontal extension veins unless there is substantial stress heterogeneity. As depth increases, increasingly high levels of fluid overpressure approaching the lithostatic load are needed to form extension veins in normal and strike–slip fault stress regimes. If the paleodepth of vein formation can be established, constraints can be placed on the degree of fluid overpressuring.

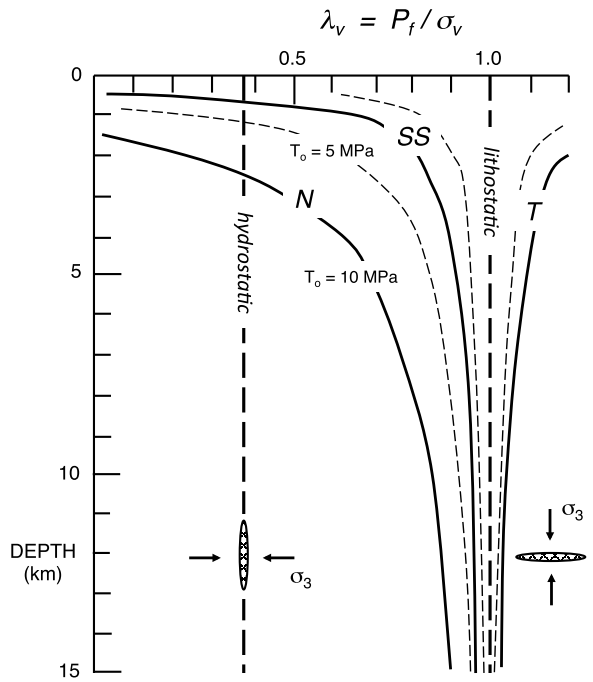

Fig. 3 Plot of the pore-fluid factor, $\lambda_v = P_f / \sigma_v$, required for hydraulic extension fracturing versus depth for the three basic stress regimes with $\sigma_v = \sigma_1$ (normal fault regime), $\sigma_v = \sigma_2$ (strike–slip fault regime with $\sigma_v = 0.5\,(\sigma_1 + \sigma_3)$), and $\sigma_v = \sigma_3$ (thrust fault regime) following the methodology of Secor (1965). Maximum differential stress limited by tensile strengths, $T_o = 5$ MPa (average sedimentary rock) and 10 MPa (competent sedimentary rock) (Lockner 1995). Adapted from Fig. 2 in Sibson (2020)

In summary, the presence of macroscopic hydrothermal extension veins: (1) defines the local orientation of σ_3 at the time of vein formation; (2) limits the level of prevailing differential stress; (3) demonstrates local attainment of the *tensile overpressure condition*; and (4) can be used to establish the degree of overpressuring provided the depth of vein formation and the stress regime can be established. Note that in several important respects this hydrofracture dilatancy, requiring dilatation of macroscopic extension fractures under high fluid pressures and low differential stress, is the inverse of microcrack dilatancy (Brace et al. 1966) developed at high differential stress and low fluid pressure levels during experimental rock deformation.

Geophysical signatures of fluid overpressure

Lowered effective confining pressure changes the physical properties of the rock mass, affecting both its seismological and electrical characteristics (Eberhart-Phillips et al. 1995). In northern Honshu, Japan, a range of geophysical observations—local occurrence of bright-spot *S*-wave reflectors, low-velocity zones, anomalously high

Vp/Vs ratios, and high electrical conductivity—support the existence of a fluid-rich ($H_2O \pm CO_2$), variably overpressured mid-crust which extends into the lower half of the upper crustal seismogenic zone, especially in the vicinity of the major fault systems (Sibson 2009; Hori et al. 2004; Hasegawa 2017). In the Himalayan foothills surrounding the 2015 **M** 7.8 Gorkha thrust rupture, the coincidence of seismic low-velocities and high electrical conductivity in a tabular zone underlying the thrust rupture (Arora et al. 2017; Rawat et al. 2014) argues for strong interconnectivity within a low-dipping, fluid-saturated mesh structure made up of subsidiary thrust and extension fractures.

Evidence of fluid-pressure cycling

Fluid inclusion studies in fault-related hydrothermal vein systems reveal ranges of homogenization temperatures consistent with cyclical pressure fluctuations during hydrothermal precipitation (Parry and Bruhn 1990; Boullier and Robert 1992; Robert et al. 1995; Henderson and McCaig 1996; Wilkinson and Johnston 1996; Parry 1998). In several cases, the range of inferred pressures alternates between near-lithostatic and near-hydrostatic values for the estimated exhumation depth.

Evidence of fault-valve activity

Supporting evidence for fault-valve activity (Fig. 4) arising from overpressured pore-fluid comes from the geological record of exhumed fault zones and from geophysical characteristics of some active fault systems.

Gold as a fluid tracer

Au–quartz mineralization has special significance as a tracer of large-volume hydrothermal flow. Laboratory measurements and field estimates suggest transport solubilities for Au of the order of ~ 10 ppb over the temperature range 300 ± 50 °C in H_2O–CO_2 fluids (Loucks and Mavrogenes 1999; Simmons and Brown 2006) whereas solubilities for quartz in pure water at 300 °C are of the order of 500 ppm. Consider, for example, the Mother Lode gold belt (> 2700 tonnes Au mined) which extends for c. 200 km along-strike in and around the Melones fault zone in the Western Sierran foothills of California (Knopf 1929; Böhlke 1999). Mineralization developed episodically from an H_2O–CO_2 mineralizing fluid in the temperature range of 250–400 °C (Böhlke 1999) during the Late Jurassic–Early Cretaceous when California was part of a subduction plate boundary. From estimates of likely transport solubilities for gold and quartz in hydrothermal fluid, Mother Lode mineralization required a

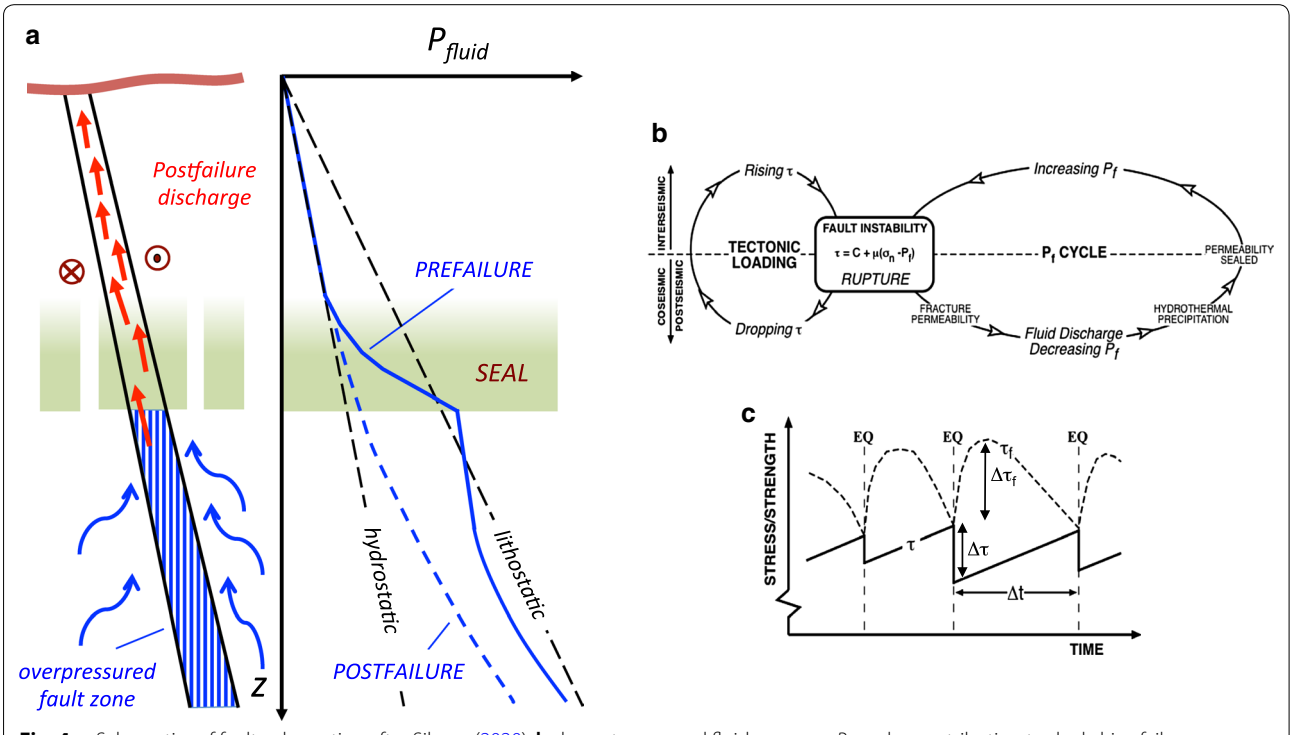

Fig. 4 **a** Schematics of fault-valve action after Sibson (2020); **b** shear stress, τ, and fluid-pressure, P_f, cycles contributing to dual-drive failure; **c** relative amplitudes of shear stress and frictional strength cycles resulting from valving action (**b** and **c** after Sibson 1992)

hydrothermal flux averaging > 1 km^3 per kilometre strike-length of the Melones fault (Sibson 2007).

Exhumed fault-valve assemblages

Fault-valve behaviour (Sibson 1981, 1990, 1992) was originally invoked to account for the occasional presence of large hydrothermal veins (quartz, calcite, etc.) hosted on faults (fault-veins), often with a clear textural record of incremental deposition (Fig. 5). The most spectacular examples are so-called mesothermal gold–quartz veins (a.k.a. orogenic lode gold) where fault-veins up to several metres thick have been mined over vertical intervals ranging up to 2 km, or so (Robert and Brown 1986; Sibson et al. 1988). For the most part, such deposits are hosted within Late Archean granite–greenstone belts or Paleozoic turbidite assemblages but younger examples in comparable rock assemblages exist (e.g. the Late Jurassic–Cretaceous Mother Lode gold belt of California (Böhlke 1999) and the early Tertiary Juneau gold belt of Alaska (Ash 2001). The hypothesis that the base of the seismogenic zone is a critical mineralizing horizon in compressional–transpressional tectonic regimes gains support from the observation that over large areas of the Superior Province in the Canadian shield, including the strongly gold-mineralized Abitibi sub-province, estimates for the depth of exhumation from metamorphic assemblages are remarkably consistent at *c.* 10 km (Carmichael 1991). Notable also is the irregular spacing of major hydrothermal vein systems along shear zone lineaments of mixed brittle–ductile character (Fig. 6) (Willman 2007; Bierlein et al. 2008; Rabeau et al. 2013; Groves et al. 2018), consistent with selective local invasion of overpressured hydrothermal fluid into the roots of major fault zones. In a typical orogenic Au–quartz deposit, a critical point is that ore grade material is distributed non-uniformly in the plane of the hosting fault structure. Dimensions of mineable ore-shoots range from hundreds of metres to a few kilometres along-strike, while elongate ore-shoots may persist down-dip for 1–2 km or more (e.g. Bierlein et al. 2008). Plausibly, this heterogeneity reflects primary flow volumes of hydrothermal fluid within the structure. This has the important implication that invasion of overpressured

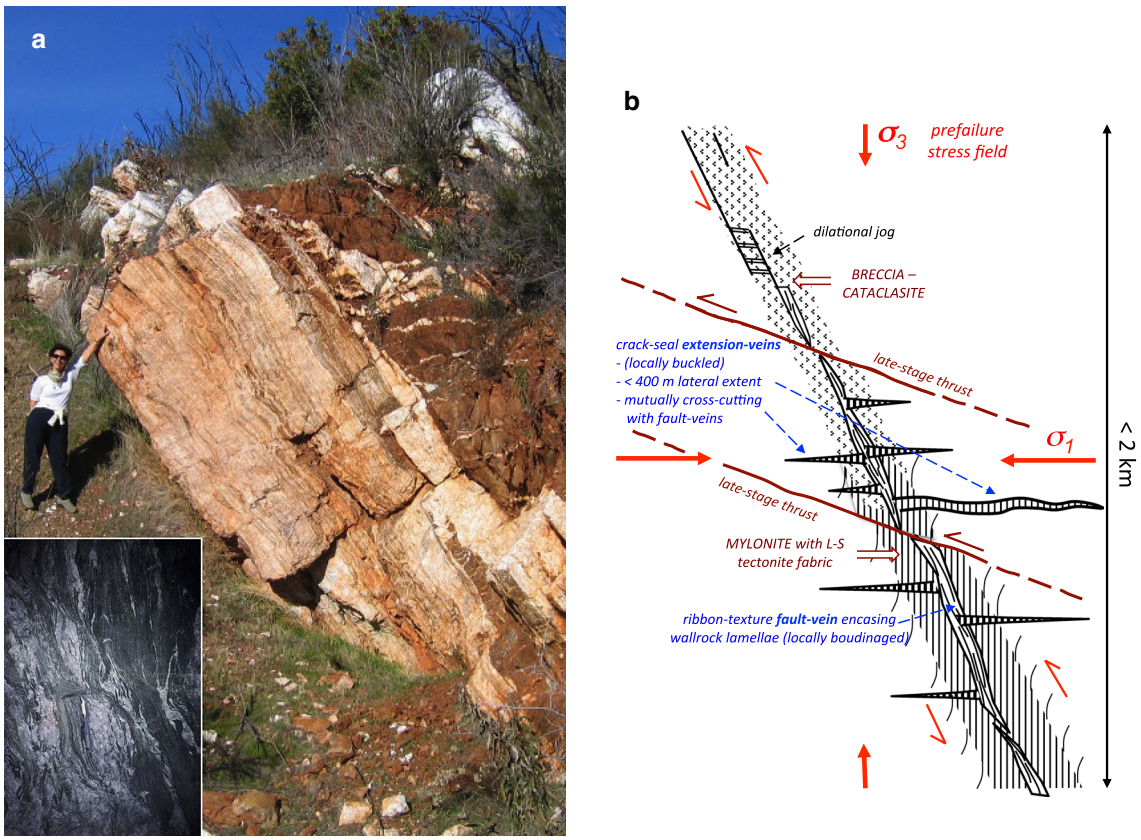

Fig. 5 **a** Mother Lode Au–quartz vein system hosted near Melones Fault, Coulterville, CA; inset at lower left shows Au–quartz veins boudinaged in steep reverse-sense ductile shear zone, Ferderber Mine, Val d'Or, Quebec. **b** Structural characteristics of fault-valve vein systems hosted on steep reverse faults (schematic and not-to-scale)

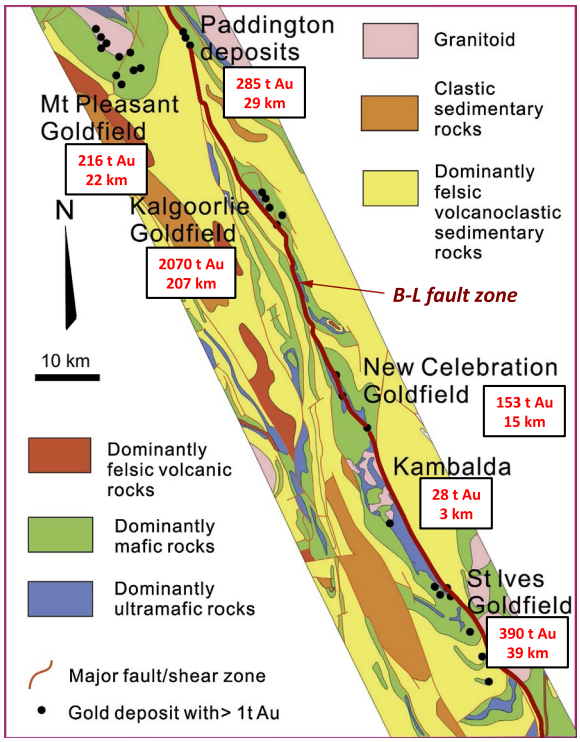

Fig. 6 Irregular distribution of major orogenic Au–quartz vein systems (> 1 tonne Au production) along the Boulder–Lefroy fault zone (B–L fault zone) transecting the Archean Yilgarn Craton of Western Australia (after Groves et al. 2018). Listed in the boxes associated with each goldfield are estimates of the total Au-endowment for each field (top) from Guj et al. (2011) (based on a compilation from Barrick Gold), and the equivalent heights of 1 km^2 columns of mineralizing fluid responsible for each field (bottom) assuming a Au/H_2O transport solubility of 10 ppb (after Fig. 5 in Sibson 2020)

hydrothermal fluids and the degree of overpressuring are heterogeneous within the fault zone.

Characteristically, the fault-veins are laminated, exhibiting 'ribbon texture' with quartz laminates interspersed with thin selvedges of wallrock. Hosting faults are of mixed 'brittle–ductile' character with a localized L–S shear zone fabric disrupted by vein fractures. Shear zone foliations (S) generally dip steeper than the bounding walls with a stretching lineation (L) raking steeply in the foliation, commensurate with reverse shear sense. Not uncommonly, fault-veins become stretched and boudinaged (inset in Fig. 5a) within the foliation. Fluid inclusion studies show that deposition from low-salinity H_2O–CO_2 fluids occurred most commonly over a depth range of 7–14 km with $270 < T < 400$ °C (Boullier and Robert 1992; Groves et al. 1998), a depositional environment corresponding roughly with the lowermost portions of currently active seismogenic zones. In many cases the hosting shear zones appear to represent the roots of high-angle reverse faults. Associated structures (Figs. 2, 5) include arrays of flat-lying extension veins that may extend tens or even hundreds of metres laterally into the wallrocks in mutual cross-cutting relationships with the fault-veins (Robert and Brown 1986; Robert et al. 1995). Some of these extension veins have been buckled during ongoing horizontal shortening. Not infrequently, the steeper shear zones are disrupted to varying extents by sets of late-stage 'Andersonian' thrust faults, typically dipping 25–30° and sometimes occurring as conjugate sets (Fig. 5).

The governing compressional stress field with $\sigma_v = \sigma_3$ (Fig. 5b) is defined by the brittle structural components. Subhorizontal extension veins developed perpendicular to the last compressive stress, σ_3, while late-stage 'Andersonian' thrust faults indicate horizontal σ_1 oriented orthogonal to the shear zone strike. Moreover, the same stress field is compatible with the evidence for predominantly reverse-shear strain across the hosting brittle–ductile shear zones with the internal foliation dipping steeper than the shear zone walls and stretch-lineations raking steeply in the foliation along with quartz slickenfibres coating the surfaces of fault-veins. Where departures from pure reverse shear have occurred, the orientations of the different structural components change accordingly.

Active fault-valve behaviour

Areas of active compressional inversion (where inherited normal faults are being reactivated under present-day horizontal compression—Fig. 6b) provide settings where geophysical indicators of reverse-fault rupturing in fluid-overpressured crust is widespread (Hasegawa et al. 2005). In northern Honshu, for example, Early Miocene rifting associated with the opening of the Japan Sea imposed a fabric of normal faults both west and east of the present magmatic arc with intensive across-arc shortening since the Late Pliocene (< 3 Ma) giving rise to active compressional inversion involving steep reverse-fault rupturing (Sato and Amano 1991). At least five $M > 6.5$ earthquakes have ruptured steep reverse inversion faults over the past 55 years (Sibson 2009). High-resolution aftershock studies show that several of these earthquakes also involved subsidiary rupturing on lower-angle thrust faults (Fig. 6a) disrupting the earlier steeper faults (e.g. Sibson 2007; Okada et al. 2012).

A broad range of seismological and electrical characteristics are consistent with strong, but locally variable, fluid-overpressuring in the lower portions (10–20 km depth) of the upper crustal seismogenic regime in Honshu. These include a plethora of bright S-wave reflectors, P- and S-wave low-velocity zones, locally high *Vp*/*Vs* anomalies in proximity to rupture hypocentres, and

high-conductivity electrical anomalies (Hasegawa et al. 2005; Hasegawa 2017; Matsumoto et al. 2005; Sibson 2009). Of particular interest is a magnetotelluric investigation of the reverse fault bounding the Shonai Plain (which last ruptured in 1894) revealing a tabular zone of high electrical conductance defining the fault to 20 km depth below the uplifted Dewa Hills (Ichihara et al. 2011). In the footwall of the fault, geochemical signatures of deep fluids with high $^3He/^4He$ ratios suggest that the rupture zone continues to discharge mantle-derived fluids to the surface along interconnected fracture permeability.

Special role of steep reverse faults in extreme valving action

Evidence that steep reverse fault zones are especially conducive to the more extreme forms of valve action comes from their role hosting orogenic Au–quartz vein systems and from the geophysical evidence for fluid overpressuring round the roots of active reverse faults with dips approaching 55–60° in areas of active compressional inversion such as northern Honshu (Sibson 2009). Such structures are unlikely to have formed at their current steep dips and have probably originated through progressive reactivation of existing fault structures (Fig. 7) (Sibson 1990). In a compressional stress field with σ_3 vertical and σ_1 horizontal (Anderson 1905), brittle shear failure of intact crust in accordance with the Coulomb criterion generally gives rise to thrust faults containing the σ_2 stress axis and dipping at 25–30° to horizontal σ_1 (Fig. 7a), reflected in the dominant peak of the dip distribution for active reverse faults (Sibson 2012). Once faults have formed, their behaviour is governed by the static coefficient of friction which, from observed dip ranges for active dip–slip faults (Colletinni and Sibson 2001; Sibson 2012), typically has a value, $\mu_s \sim 0.6$, towards the lower end of the experimentally determined range for hard-rock friction (Byerlee 1978). For an existing fault lacking cohesive strength the criterion for reactivation reduces to:

$$\tau = \mu_s \sigma_n' = \mu_s (\sigma_n - P_f), \tag{4}$$

which can be rewritten in terms of the ratio of principal stresses as:

$$\sigma_1'/\sigma_1' = (\sigma_1 - P_f/\sigma_3 - P_f) = (1 + \mu_s \cot\theta_r)/(1 - \mu_s \tan\theta_r) \tag{5}$$

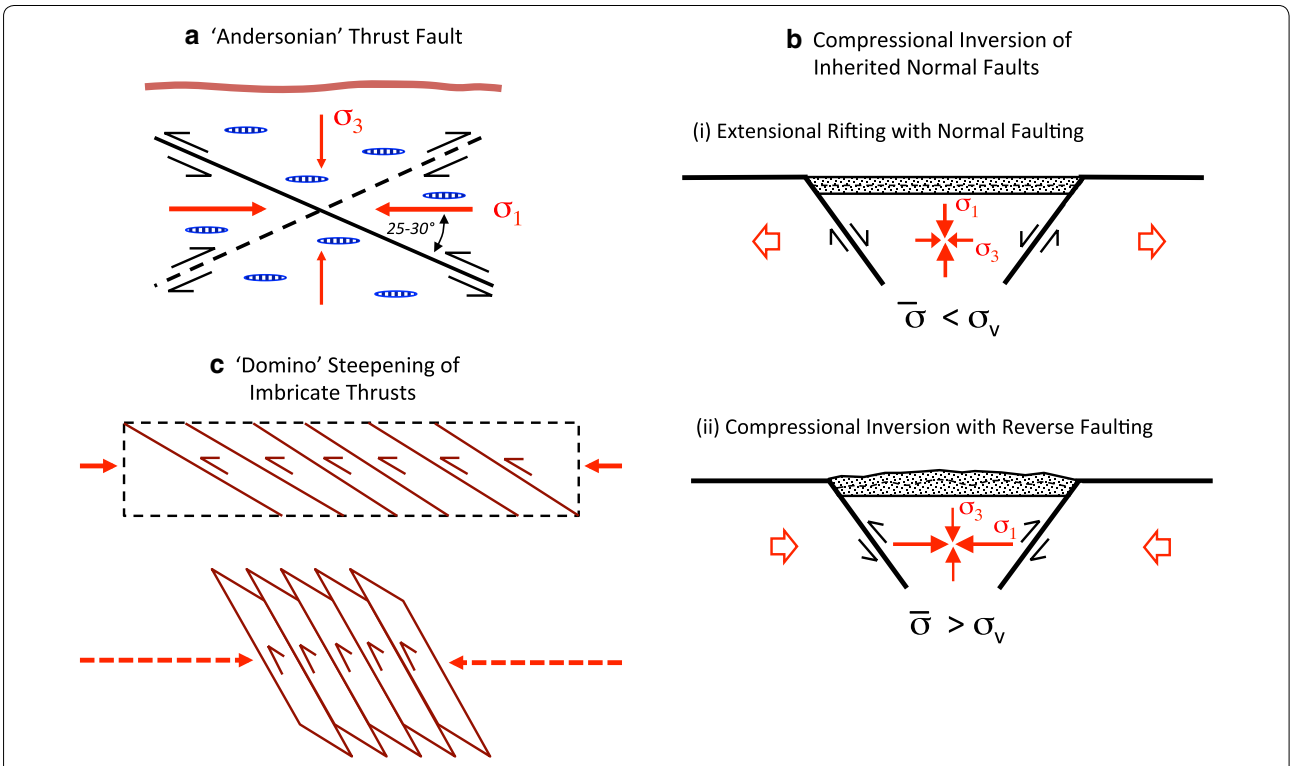

Fig. 7 **a** Initiation of an 'Andersonian' thrust fault dipping 25–30° within homogeneous, isotropic intact crust under horizontal compression; **b** steep reverse fault arising from compressional inversion of inherited normal faults; **c** steep reverse faults as a consequence of domino-steepening during progressive crustal contraction

for faults containing the σ_2 axis and oriented at a reactivation angle, θ_r, to σ_1, (Sibson 1985). This 2-D reactivation analysis serves as a measure of the ease of fault reactivation for different orientations. It has a minimum value when the fault is optimally oriented for reactivation at $\theta_r^* = 0.5\ \tan^{-1}(1/\mu_s)$ to σ_1. As θ_r increases or decreases from θ_r^*, the stress ratio required for reactivation increases towards infinity as $\theta_r \rightarrow 0$ or when $\theta_r \rightarrow 2\theta_r^* = \tan^{-1}(1/\mu_s)$ (Sibson 1985). For $\mu_s = 0.6$, optimal reactivation with $\sigma_1'/\sigma_3' = 3.12$ occurs when $\theta_r = 29.5°$ and frictional lock-up when $\theta_r = 59°$. Reactivation in the field of severe misorientation ($\theta_r > 2\theta_r^*$) is still possible but only when the *tensile overpressure condition* ($\sigma_3' < 0$ or $P_f > \sigma_3$) is met. Approaching frictional lock-up, fault reactivation becomes increasingly sensitive to small increases in fluid pressure (ΔP_f) so that reshear of steep reverse faults in such circumstances is likely to be predominantly fluid-driven (Sibson and Ghisetti 2018).

In a compressional regime with $\sigma_v = \sigma_3$, the effective vertical stress at a depth, z, is $\sigma_v' = \rho gz(1 - \lambda_v)$ where ρ is average rock density and g is gravitational acceleration. Combined with Eq. 5, this yields an expression for the level of differential stress needed to reactivate a cohesionless reverse fault with pure reverse-slip:

$$(\sigma_1 - \sigma_3) = \mu_s \left[(\tan\theta_r + cot\theta_r) \big/ (1 - \mu_s \tan\theta_r) \right] \rho gz(1 - \lambda_v) \quad (6)$$

relating the required level of differential stress to the friction coefficient, μ_s, the orientation of the reverse fault, θ_r, with respect to σ_1, the depth, z, and the pore-fluid factor, λ_v. This expression likewise has a minimum value when the fault is optimally oriented for reactivation at $\theta_r^* = 0.5\ \tan^{-1}(1/\mu_s)$ to σ_1, with the required differential stress tending to infinity as θ_r approaches 0 or $2\theta_r^*$, the angle of frictional lock-up (Sibson 1985, 1990).

Principal scenarios for the development of steep reverse faults with dips > 45° are illustrated in Fig. 7 (Sibson 1990, 2012). Figure 7a illustrates an 'Andersonian' thrust fault initiating through Coulomb shear failure of homogeneous isotropic crust under horizontal compression (Anderson 1905). Figure 7b illustrates compressional inversion of inherited normal faults when crust previously rifted under horizontal extension is subjected to horizontal compression. Pure reverse slip on steep faults may then be induced when compression is coaxial with former extension. Non-coaxial inversion leads to reverse-oblique slip on the inherited faults (Sibson and Ghisetti 2018). Another possible scenario (Fig. 7c) involves the continued shortening, for example in a collisional setting, of a suite of initially low-dipping 'Andersonian' thrust faults which undergo progressive 'domino steepening' until they approach frictional lock-up as their dips increase towards 60° (Sibson and Xie 1998). An instructive example is the collision zone between the Kurile fore-arc and the NE-Japan arc in the Hokkaido Corner where an imbricate stack of moderately to steeply ENE-dipping reverse faults remains active to dips approaching 60° and beyond within steep zones of high electrical conductivity likely diagnostic of extreme overpressuring (Kita et al. 2012; Ichihara et al. 2016). In such settings it is also likely that new, optimally oriented thrust faults are forming in competition with the steep misoriented reverse faults (Sibson 2012).

Lithostatically overpressured fluid reservoirs

In a uniform compressional stress regime with ($\sigma_v = \sigma_3$), the maximum sustainable overpressure is governed by the formation of subhorizontal hydraulic extension fractures, requiring supralithostatic overpressure to dilate vertically (i.e. $P_f = \sigma_v + T_o$, or $\lambda_v > 1.0$). However, the presence of existing cohesionless faults that are favourably oriented for reactivation inhibits the formation of hydraulic extension fractures because the faults then tend to reactivate in shear before the criterion for hydraulic extension fracturing can be attained (Sibson 2000, 2003). Dilatant hydraulic extension fractures resulting from the build-up of fluid overpressure are therefore restricted to: (i) intact crust retaining cohesive strength; (ii) crust where existing faults have regained cohesive strength through hydrothermal cementation, etc.; and (iii) crust where existing faults are severely misoriented for reactivation (i.e. oriented at > *c.* 60° to σ_1). In this last circumstance, there is abundant field evidence that hydraulic extension fractures can develop in the vicinity of existing faults that are severely misoriented for reactivation (Sibson et al. 1988; Robert et al. 1995). Depending on the tensile strength of a sealing horizon, such arrays may extend over vertical intervals approaching 1 km or so (Sibson and Scott 1998).

Damang gold mine, Ghana (Fig. 8), provides an example of an exhumed vein swarm where a compressional fault–fracture mesh containing subhorizontal Au-bearing quartz veins disrupts a sequence of Paleoproterozoic metasediments and metavolcanics, folded and reverse-faulted in an upright, gently NNE-plunging antiform–synform sequence (Tunks et al. 2004). Likewise at Minas da Panasqueira, Portugal, an extensive (3 km × 5 km) swarm of subhorizontal W ± Sn-bearing quartz extension veins mined over a vertical interval of ~ 1 km is associated with a granitoid cupola intruding a Hercynian metamorphic assemblage (Foxford et al. 2000). Individual veins up to a metre or so in thickness have dimensions ranging up to *c.* 1 km or more, but the entire swarm covers an area in excess of 15 km^2. While some of the veins retain crack-seal textures recording incremental growth, others have open-space filling textures suggesting that the extension

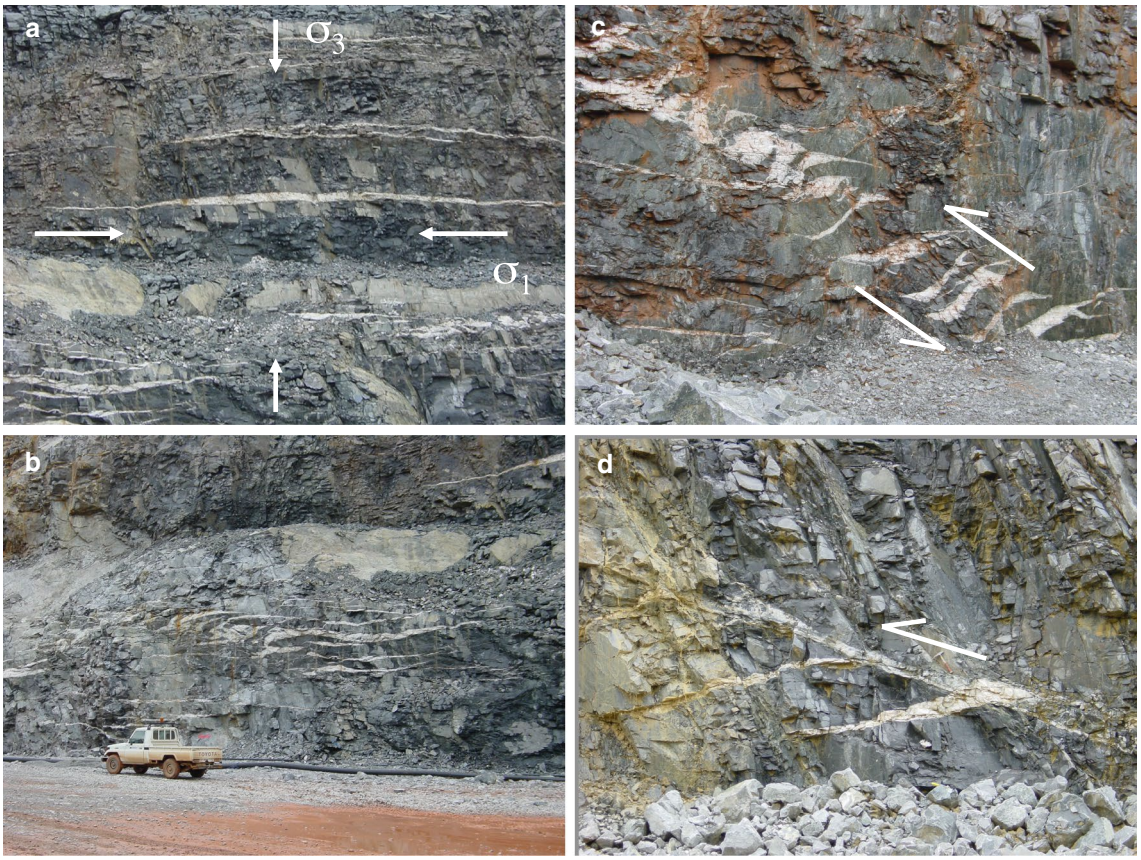

Fig. 8 Au-bearing quartz vein swarm at Damang Gold Mine, Ghana (from Tunks et al. 2004): **a** array of subhorizontal extension veins cutting steeply dipping Paleoproterozoic meta-sandstones; **b** subhorizontal extension veins locally evolving into a thrust-sense tension-gash shear zone under horizontal compression; **c** thrust-sense sigmoidal tension-gash shear zone; **d** mineralized thrust fault cutting through tension-gash shear zone (photographs courtesy of Andrew Tunks)

fractures were held agape (> 100 mm) by fluid overpressure for substantial time periods (Foxford et al. 2000).

Mid-crustal overpressuring on a regional scale is likely to be occurring in the Tohoku region of northern Honshu (Fig. 9) where horizontal regional σ_1 trajectories lie approximately orthogonal to the magmatic arc along the Ou Backbone Range which is flanked by active, inward-dipping, steep reverse faults (Hasegawa et al. 2005; Hasegawa 2017). Bright flat-lying *S*-wave reflectors are concentrated at depths of 10–20 km in and around the base of the seismogenic zone below an area approximately 200 km × 50 km (Hori et al. 2004; Hasegawa 2017). A reasonable inference is that the reflectors arise from fluid reservoirs, made up of arrays of subhorizontal extension fractures pressurized by magmatic or hydrothermal fluid (cf. Fig. 8). Regional development and inflation of such magmatic and hydrothermal water sills would be facilitated by the severely misoriented character of the flanking steep reverse faults, oriented at or beyond frictional lock-up.

Given the concentration of reflectors in the lower seismogenic zone, the most favoured sites for extensional vein swarms would likely be in the dilational quadrant abutting the down-dip termination of steep reverse-slip ruptures, developing in a manner akin to wing-cracks (cf. Willemse and Pollard 1998) (Fig. 10a). Robert et al. (1995) have described Au–quartz veins occupying apparent wing-cracks at the down-dip terminations of reverse faults. On a larger scale, a lithostatically overpressured mesh of extension fractures developed prefailure in the basal hanging-wall of a steep reverse fault near the base of the seismogenic zone would form a substantial reservoir of overpressured fluid available for discharge into and up the reverse fault rupture zone postfailure (Fig. 10). Note further that estimated temperature ranges for the overpressured hydrothermal fluids responsible for orogenic gold mineralization (e.g. 250–400 °C for the Mother Lode belt—Böhlke (1999)) are consistent with their being derived from a reservoir developed near the base of the upper crustal seismogenic zone.

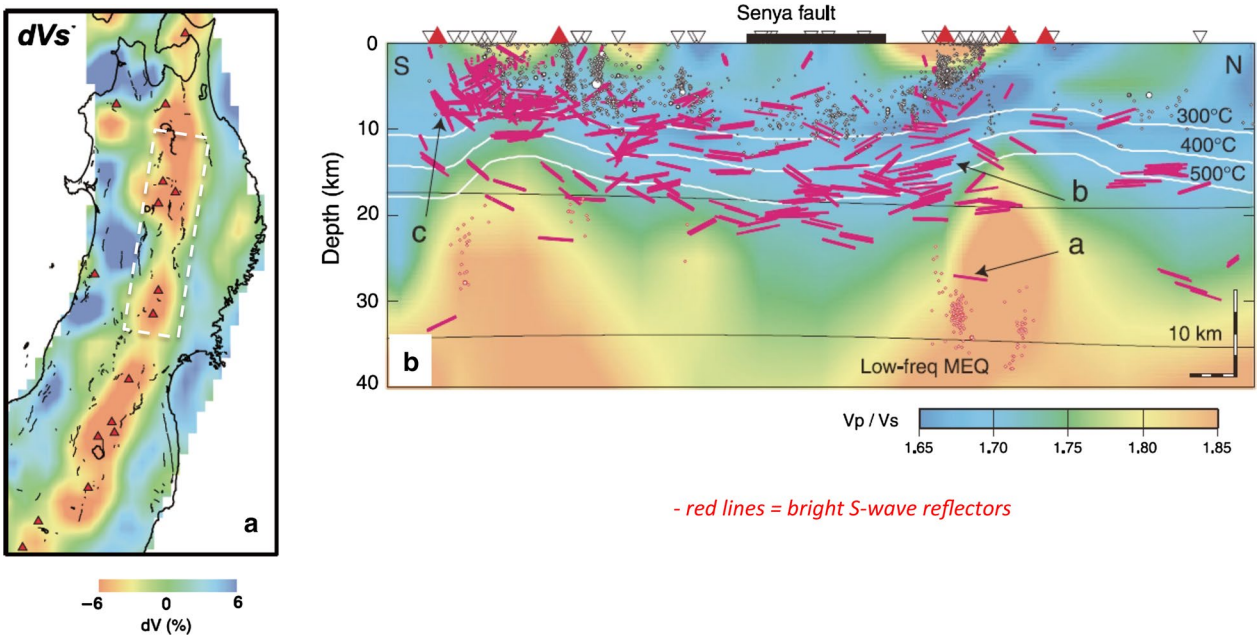

Fig. 9 **a** Map of northern Honshu with volcanic front in Ou Backbone Range (flanked by inward-dipping reverse fault systems) delineated by lowered *dVs*; **b** N–S longitudinal section along the Ou Backbone Range (white rectangle) showing bright S-wave reflectors (red lines) in relation to the depth of the seismogenic zone, estimated isotherms, and variations in *Vp/Vs* (from Hasegawa 2017)

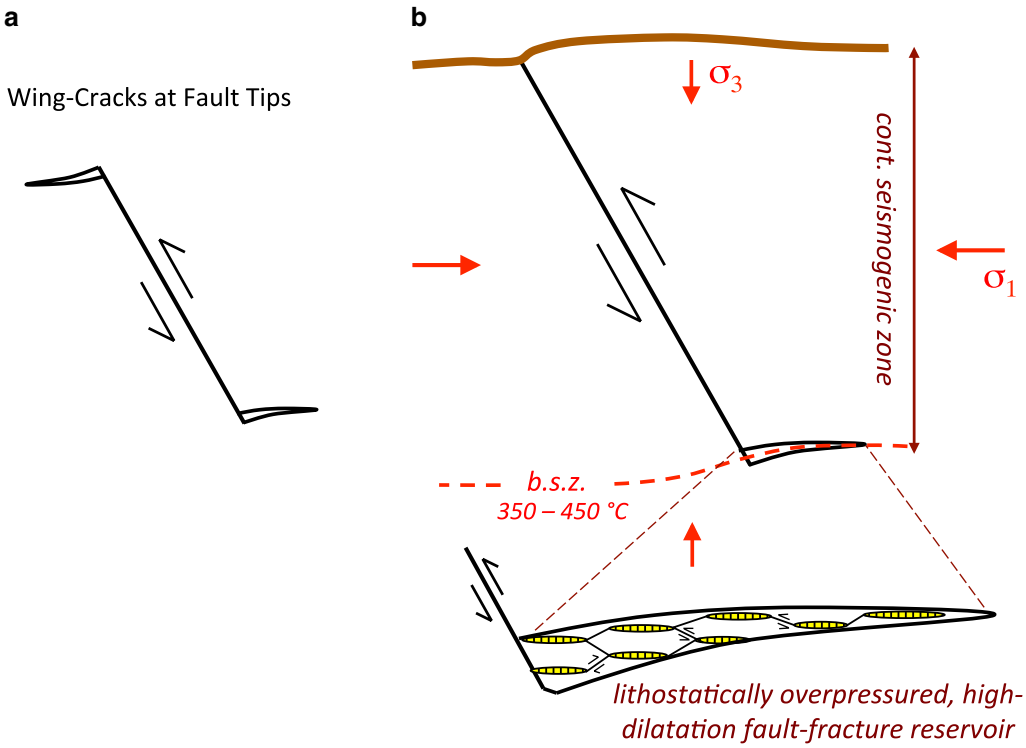

Fig. 10 **a** Development of wing-cracks at the tip of a steep reverse fault under horizontal compression within intact crust (cf. Willemse and Pollard 1998); **b** hypothetical development of an overpressured fluid reservoir near the base of the upper crustal seismogenic zone, in the dilatational quadrant associated with the termination of a steep reverse fault

Major versus minor valving action

In terms of economic mineralization, valving action is significant only if the fluid volume discharged per fault rupture (earthquake) is large. As previously noted, conservative estimates suggest that major fault-hosted veins along the Melones Fault in the Mother Lode gold belt of California result from an integrated hydrothermal discharge in excess of 1 km^3 per kilometre strike-length of the fault, with the fluid volume per discharge likely to be several orders of magnitude lower. However, this may be the exception rather than the rule and only develop under special circumstances. In low-porosity rocks, loss of comparatively small fluid volumes through valving action can still bring about large increases in effective stress and, hence, frictional strength (Sibson 1992).

Tectonic settings for fault-valve activity

The most favourable tectonic settings for developing fluid overpressures conducive to fault-valve activity seem likely to be compressional and transpressional regimes because of their heightened ability to contain fluid overpressure when $\sigma_v = \sigma_3$ (Sibson 2003). Such regimes also tend to be *load-strengthening* (Sibson 1993) so that increasing differential stress through each loading cycle to failure is accompanied by increases in mean stress and pore-fluid pressure through poroelastic coupling (Simpson 2001). There are two tectonic settings where extreme fault-valve behaviour giving rise to intermittent discharge of large fluid volumes seems especially likely. First, extreme valving action becomes probable in areas undergoing active compressional inversion where existing inherited faults are poorly oriented for reactivation (Fig. 7b), contributing to fluid redistribution (Turner and Williams 2004). Second, ongoing bulk shortening in subduction forearcs and zones of continental collision may lead to progressive domino-steepening (Fig. 7c) of initially low-angle thrusts towards frictional lock-up as steep reverse faults with dips $\rightarrow 60°$ (Sibson and Xie 1998), also providing an environment conducive to extreme fault-valve action. Such seems to be the case in the Hokkaido Corner where the Kurile forearc is colliding with the NE-Japan arc (Kita et al. 2012). In both these settings, finite deformation involves crustal thickening by reverse faulting and upright folding with cleavage development (involving significant diffusive mass transfer over the temperature range 200–400 °C), all contributing to prograde metamorphism and dewatering at depth. In transpressional settings involving bulk horizontal shortening there will be a general tendency for sliding surfaces to become progressively steepened and misoriented for frictional reactivation. Existing reverse faults will be progressively steepened while strike–slip faults will be rotated towards the flattening plane (Tikoff and Greene 1997), all contributing to an environment increasingly favourable to fault-valve action.

In predominantly pelitic assemblages, major fluid release occurs at the onset of greenschist facies metamorphic conditions (c. 350 ± 50 °C) and also at the greenschist–amphibolite facies boundary (c. 550 ± 50 °C) (Fyfe et al. 1978) with widespread recognition that in such settings $P_f \sim P_l$ (i.e. $\lambda_v \sim 1.0$) (Etheridge et al. 1984). Metamorphic dehydration reactions in the mid-crust may therefore contribute to brittle failure through generation of fluid overpressure (cf. Hacker 1997; Ague et al. 1998). Fluid overpressuring is unlikely to be uniform but may be focused upwards by 'antiformal domes' developed in folded turbidite sequences (Fig. 11a, b) enclosing overpressured reverse-fault systems that promote hydrothermal mineralization through valve action (e.g. Cox et al. 1991; Willman 2007). Downwards flaring ductile shear zones may also funnel the ascent of metamorphic fluids contributing to the 'patchy' character of mineralization (Fig. 11c).

Thermal structure within zones of convergence and intense crustal shortening depends on a complex array of factors including the distribution of radiogenic heat-producing material, the rate of convergence with the possibility of shear heating along thrust interfaces, vertical stretching, and the rate of erosional denudation (Graham and England 1976; Oxburgh and England 1980; England and Thompson 1984). A general expectation, however, is that crustal thickening by thrust faulting tends to depress the overall geothermal gradient whilst raising the temperature in the top of the underthrust slab (Graham and England 1976) so that underthrust material, commonly with high porosity and fluid content, undergoes prograde metamorphism and fluid release.

Areas of active transpression are also notably prone to 'flake tectonics' (Oxburgh 1972), where detachment of upper crustal 'flakes' is consistent with rheological strength profiles suggesting dramatic weakening below the seismogenic zone (Sibson 1984). Development of fluid-rich, flat-lying, thrust-sense shear zones is then likely in the mid-crust immediately below the upper crustal seismogenic zone. Possible 'live' examples include the highly reflective NNE-dipping shear zone at 18–23 km depth underlying the San Gabriel mountains adjacent to the San Andreas fault (Ryberg and Fuis 1998), and the tabular, electrically conductive, low-velocity zone underlying the 2015 **M** 7.8 Gorkha thrust rupture in the frontal Himalaya (Arora et al. 2017; Rawat et al. 2014).

Seismic cycle incorporating fault-valve behaviour

Based on the geological and geophysical evidence for fault-valve action, likely effects at different levels within the crustal seismogenic zone can be envisaged

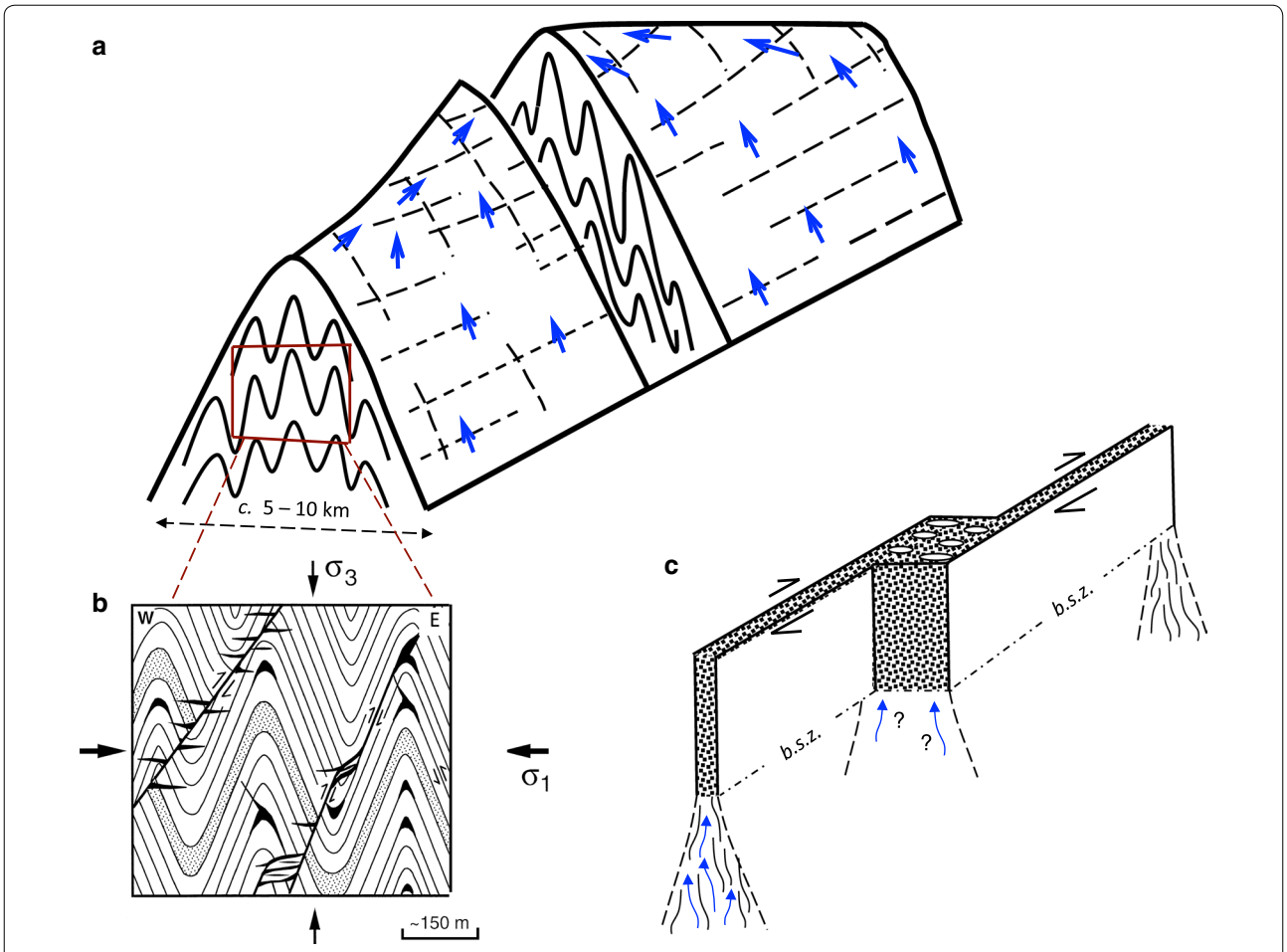

Fig. 11 **a** Schematic of hydrothermal fluid flow (arrows) inferred for an amplifying anticlinorial dome structure within the Upper Ordovician turbidite sequence of the Bendigo–Ballarat area of the Lachlan fold-belt of Victoria, Australia (after Cox et al. 1991; Willman 2007); **b** structural and inferred stress controls on Au–quartz vein systems (black) developed within similar upright fold structures in the Lachlan fold-belt (after Cox 1995; Sibson and Scott 1998; Willman 2007; Sibson 2020); **c** schematic of dextral strike–slip fault zone with a local dilational jog: fluid focusing occurs within ductile shear zones which flare outwards below the base of the seismogenic zone (b.s.z.) and within the enhanced permeability of the dilational stepover which acts as a pipe conduit

for different stages of the seismic cycle for large earthquakes. Note that a high level of conjecture is involved! For ease of reference, the upper crustal seismogenic zone is assumed to extend to 15 km depth (equating to the onset of greenschist facies metamorphic conditions at c. 350 °C) and is subdivided into upper (0–5 km), middle (5–10 km), and lower (10–15 km) portions. Bear in mind that these subdivisions are arbitrary and that effects within the seismogenic zone also depend on sub-seismogenic processes such as metamorphic fluid release over lengthy time periods.

INTERSEISMIC—over the interseismic period (typically 10^2–10^4 years) steadily rising differential stress from differential plate motion increases shear stress acting on frictionally locked faults throughout the full depth of the seismogenic zone. In compressional–transpressional tectonic settings which are inherently load-strengthening (Sibson 1993), increasing shear stress is coupled to increases in both mean stress and fault-normal stress. However, these strengthening effects may be counteracted by progressive infiltration of overpressured porefluids from metamorphic dehydration at subseismogenic depths, lowering effective normal stress, $\sigma_n' = (\sigma_n - P_f)$, and hence, fault frictional strength in the lower seismogenic zone (Fig. 12).

PRESEISMIC (day to years?)—incipient shear failure with accelerating shear strain-rate. Percolation may allow overpressuring to extend upwards through the middle seismogenic zone or above. Local attainment of the tensile overpressure condition ($P_f > \sigma_3$) where existing

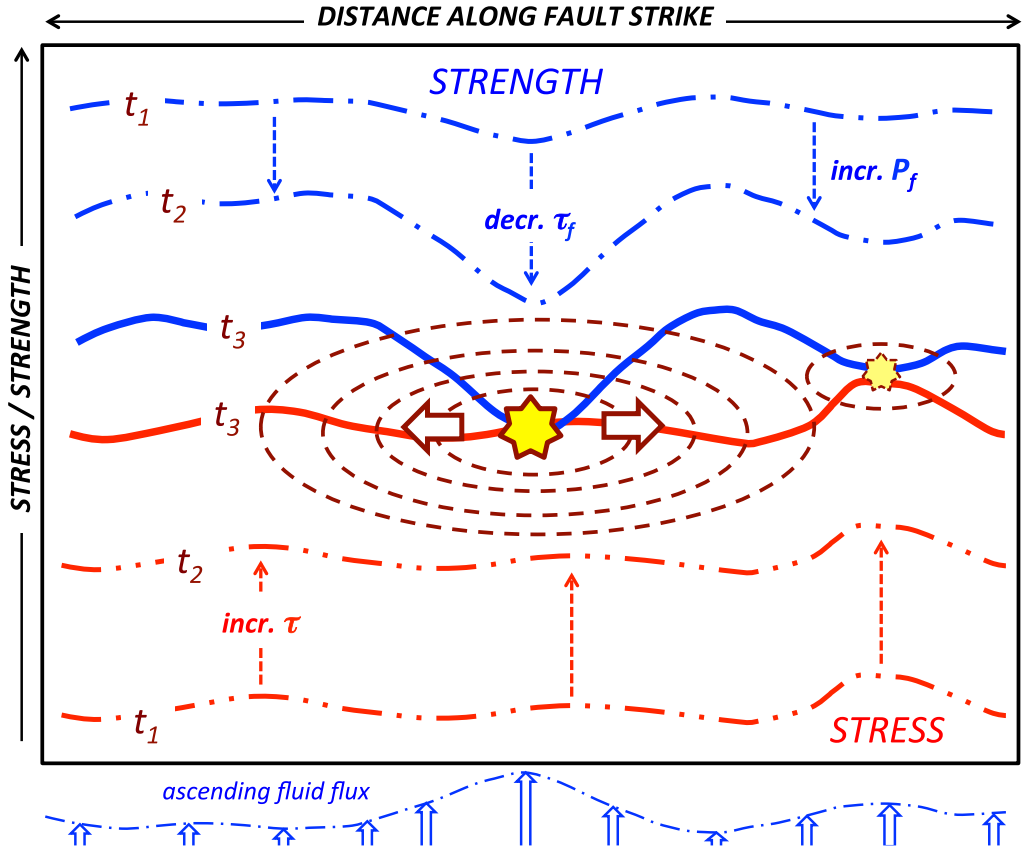

Fig. 12 Schematic illustrating time-varying stress and strength leading to the dual-driven failure of a crustal fault subjected to an ascending overpressured fluid flux at times, t_1, t_2, and t_3 (mainshock and aftershock hypocentres denoted by yellow stars; nested ellipses illustrate growth of mainshock rupture) (adapted from Fig. 8 of Sibson (2020))

faults have restored cohesive strength (perhaps through hydrothermal cementation) or are severely misoriented for frictional reactivation allows hydrofracture arrays to develop and activate (Sibson 2017). Inflation of overpressured fluid reservoirs around the base of the seismogenic zone is especially likely around the brittle roots of severely misoriented faults. Linkage to existing faults in distributed fault–fracture meshes gives rise to diffuse microseismicity (Sibson 1996; Cox 2016).

COSEISMIC (< 200 s)—initiation of mainshock rupture from a combination of rising shear stress and lowered frictional strength in the lower seismogenic zone (Fig. 12). Rupture propagation is accompanied by stress redistribution with an overall drop in shear stress. Fault zone permeability is enhanced dramatically but heterogeneously, promoting upwards fluid discharge. Progressive fluid loss from rupture zone and dilatant reservoirs lowers overpressure, increasing fault frictional strength.

POST-SEISMIC ($0.1–10^2$ years)—long duration aftershock activity accompanies prolonged fluid discharge with progressive fault healing involving hydrothermal cementation and decreasing fault permeability (e.g. Silvio et al. 2007). Nonetheless, fluid interconnectivity in pore and fracture space may persist for lengthy time periods throughout the aftershock phase (e.g. Miller et al. 2004).

Relevant geophysical and geological observations

Geophysical observations

Seismic P- and S-wave velocities vary with rock type, confining pressure, and fluid content (Christensen 1989; 1996). At constant confining pressure increased pore-fluid pressure decreases both P-wave and S-wave velocities, the latter more than the former, so that overall the *Vp/Vs* ratio (equating to elevated Poisson's ratio) increases. Diagnostics of overpressured aqueous fluid occupying pore and/or fracture space in the crust therefore include anomalously lowered P- and S-wave velocities and an elevated *Vp/Vs* ratio, though this may also be affected by the geometry of pore and/or fracture space (Eberhart-Phillips et al. 1995; Takei 2002). For continental crust, average Poisson's ratio is 0.265 corresponding to $Vp/Vs = 1.77$ (Christensen 1996). This compares

with a Poisson's ratio of 0.300 ($Vp/Vs = 1.87$) for oceanic crust and 0.270 ($Vp/Vs = 1.78$) for the sub-Moho mantle beneath central Honshu, Japan. For continental crust and the sub-Moho mantle, regions with $Vp/Vs > 1.80$ are thus potentially fluid-overpressured. However, the compositional and structural heterogeneity of continental crust has to be kept in mind.

The presence of pervasive pore/fracture fluid also lowers bulk electrical resistivity though this may also be caused by metallic sulphides or graphite distributed through the rock-mass. Strong interconnectivity of pore fluid throughout the rock-mass is, however, only likely to arise when $P_f \rightarrow \sigma_3$, generally requiring near-lithostatic fluid overpressures ($\lambda_v \rightarrow 1.0$). The combination of lowered seismic velocities and high Vp/Vs anomalies coincident with high electrical conductivity therefore provides the strongest diagnostic for defining crustal and subcrustal domains with elevated fluid overpressure in pore and/or fracture space (Eberhart-Phillips et al. 1995).

Tomographic investigations of the velocity structure of seismogenic crust in compressional/transpressional settings have shown: (1) A tendency for large crustal earthquakes to be associated with extensive ($100 < L < 200$ km) low-velocity zones (especially low Vs) in the mid-to-deep crust and underlying upper mantle (Okada et al. 2010, 2012); and (2) that rupture nucleation sites tend to be associated with elevated but more localized Vp/Vs anomalies ($10 < L < 30$ km) (e.g. 1995 **M** 6.9 Kobe earthquake (Zhao and Negishi 1998); 2000 **M** 6.7 Western Tottori earthquake (Zhao et al. 2004); 2001 Bhuj **M** 7.6 earthquake (Kayal et al. 2002); 2004 **M** 6.8 Mid-Niigata earthquake (Wang and Zhao 2006); 2008 **M** 7.2 Iwate-Miyagi-Nairiku earthquake (Okada et al. 2012); 2016 **M** 7.3 Kumamoto earthquake (Wang et al. 2018)).

The **M** 7.8 Kaikoura, New Zealand earthquake (11.02 on 13/11/2016 UTC) was a complex transpressional multi-rupture with 20 + surface breaks involving a mixture of reverse and both dextral and sinistral strike–slip (Hamling et al. 2017; Litchfield et al. 2018). Rupturing occurred over a total strike-length approaching 200 km, propagating SW → NE along the northeastern coast of New Zealand's South Island. A regional tomographic analysis of the Marlborough strike–slip fault system conducted prior to the event (Eberhart-Phillips and Bannister 2010) revealed a chain of high Vp/Vs anomalies at c. 15 km depth along the coast underlying much of the subsequent rupture zone, suggesting that overpressured fluids were likely involved in the nucleation and propagation of this complex multi-rupture.

Geological observations

Accepting that the base of the continental seismogenic zone broadly correlates with the onset of greenschist facies metamorphic conditions at T > *c.* 350 °C, lower portions of the brittle carapace to a prograding metamorphic system should equate roughly with the lower seismogenic zone. Consider, for example, the Otago Schist belt of southern New Zealand, embracing the Jurassic collisional suture between the Caples and Torlesse accretionary terranes (Mortimer 1993, 2003). The belt occupies an area measuring approximately 250 km × 160 km made up of greenschist and amphibolite facies assemblages with a penetrative foliation resulting from polyphase ductile deformation that defines a broad antiformal arch trending NW–SE. Foliation is flat-lying in the crest of the arch with dips increasing progressively to the NE and SW where the schists are flanked by a brittle subgreenschist carapace several kilometres thick (Mortimer 1993) made up of prehnite–pumpellyite facies metagreywackes in which bedding is largely preserved with little obvious flattening of clastic grains in the sandstones, the product of low-grade metamorphism at temperatures of 250–350 °C. Deformation within the metagreywackes is highly variable but locally comprises a criss-crossing mesh of planar extension fractures together with minor faults and their conjugates, all with hydrothermal infills (quartz + prehnite ± epidote ± pumpellyite ± calcite) distributed throughout substantial volumes of hydrothermally altered rock (Bishop 1994; Spörli and Anderson 1980; De Ronde et al. 2001). Sparse Au–quartz mineralization is also locally present within such prehnite–pumpellyite metagraywackes (Becker et al. 2000). These characteristics are consistent with fluid-driven deformation arising from patchy infiltration of near-lithostatically overpressured fluids from depth.

The field relationships thus support the hypothesis that the prehnite–pumpellyite metagraywacke assemblages represent exhumed portions of a former lower seismogenic crust infiltrated by fluids derived from prograde metamorphism at greater depths.

Relevance to contemporary earthquakes

An hypothesis has been advanced for the development of earthquake preparation zones as a consequence of fault-valve action where fault failure is *dual-driven* by a combination of stress accumulation and rising fluid-pressure affecting frictional strength in the lower seismogenic zone and in the underlying shear zones which may continue downward into the upper mantle. Irrespective of the mode of faulting, any earthquake rupture disrupting a low-permeability seal capping an overpressured portion of the crust may give rise to postfailure discharge through fault-valve action. The magnitude of the ensuing discharge likely varies with the faulting mode and size of the rupture, the dimensions of the overpressured reservoir, the degree of overpressuring, and fracture

interconnectivity within the reservoir. Geological evidence coupled with mechanical analyses suggest, however, that steep reverse faults that are poorly oriented for frictional reactivation in compressional regimes, have the greatest potential for large postfailure discharge through valving action (Sibson 1990, 2014).

Questions remain, however, as to how widespread this process is and whether recognizable preparation zones develop when valve action occurs in less than its more extreme forms associated with steep reverse faults. Systematic, rigorous evaluation employing combined seismological and electrical sounding is needed to test how widespread these associations are in different tectonic settings and, importantly, to see whether they exhibit time-dependent behaviour before and after large earthquakes.

There is also a clear need for improved quantification of the fluid budgets associated with areas of reduced seismic velocity and elevated *Vp/Vs* as well as quantifying fluid discharge for valving activity in different tectonic settings. Another potentially fruitful line of inquiry would involve geochemical investigation of post-seismic fluid discharges. Prolonged sampling throughout aftershock periods is needed to ensure that deep-derived, rather than displaced high-level fluids are sampled. Example of areas where fault-valve activity could be investigated with discharge events potentially tied to seismic slip increments include the seismically and diapirically active front of the Apennine fold-thrust belt in northern Italy (Bonini 2007; Bonini et al. 2016), and overpressured geothermal systems in compressional tectonic settings such as the Cooper Basin geothermal field of South Australia (Holl and Barton 2015).

One expected consequence would be that nucleation sites for fluid-driven rupture would remain fixed for substantial time periods. An important question, therefore, is whether there are preferential sites for the nucleation of large ruptures and whether they remain fixed with time? There is considerable evidence from paleoseismological studies for repeating large earthquakes (Sieh 1996) but it is unclear whether successive 'characteristic' earthquakes always nucleate at the same site, though this seems likely to have been the case for the 1922, 1934, and 1966 events in the Parkfield, California series of moderate ($\mathbf{M} \sim 5.5$) strike–slip ruptures (Bakun and Lindh 1985).

A related issue is whether there are distinguishing characteristics for mainshock ruptures resulting from predominantly fluid-driven failure? As one possible example, consider the 1989 **M** 6.9 Loma Prieta earthquake which involved dextral-reverse-slip on an ~ 70° dipping plane adjacent to the San Andreas fault, with the rupture initiating at the unusually large (for the northern San Andreas fault) focal depth of 19 km (Spudich 1996). Locally elevated fluid overpressure and initiation of fluid flow at hypocentral depths could account for this local deepening of the seismogenic zone by > 5 km (Sibson 1984), and might also help explain a precursory magnetic disturbance starting 3 h before the earthquake (Fraser-Smith et al. 1995), a reported precursory increase in surface stream flow an hour before the mainshock (Roeloffs 1995), as well as evidence in the form of highly diverse aftershock focal mechanisms for near-total release of shear stress over the mainshock rupture, consistent with a highly overpressured fault (Zoback and Beroza 1993). A comparable diversity of aftershock focal mechanisms (again implying near-total relief of shear stress) is associated with the 1952 **M** 7.7 Kern County earthquake (Castillo and Zoback 1995) involving varying proportions of sinistral and steep reverse slip along the White Wolf fault in the southern San Joaquin Valley of Central California from a rupture initiating at c. 18 km depth. Interestingly, this earthquake was associated with significant post-seismic fluid discharge ($> 10^7$ m^3 over 2 months) from the crystalline hanging-wall of the fault (Briggs and Troxell 1955; Sibson 1981).

Important lessons may also be learned from variations in the style of seismicity induced by injection of overpressured fluid (Ellsworth 2013). While much seismicity induced by fluid injection at depth tends to be diffuse and distributed through substantial rock volumes, akin to swarm seismicity (cf. Cox 2016), there are instances where induced earthquake activity more nearly approximates natural mainshock–aftershock sequences. One such example is the 2017 $\mathbf{M}_w$ 5.5 Pohang, Korea, earthquake triggered by enhanced geothermal stimulation at ~ 4 km depth in a compressional stress field (Ellsworth et al. 2019). This earthquake involved dextral–reverse slip on an existing fault with a rupture dimension of ~ 5 km, extending well beyond the area of fluid injection. It may be that the differing seismic style depends on whether or not localized fluid overpressures have direct access to a mature uninterrupted planar fault structure (cf. Galis et al. 2017). In such circumstances, ruptures may propagate well beyond the areas of localized fluid overpressure associated with their nucleation as illustrated schematically in Fig. 12.

Summary and conclusions

Release of H_2O–CO_2 fluids at near-lithostatic overpressure from prograde metamorphism consequent on crustal thickening is an inevitable accompaniment of compressional–transpressional tectonics. Ascent of such overpressured fluids is dominated by channel flow along faults and ductile shear zones where permeability is continually renewed by active deformation. Flow

is non-uniform with portions of fault zones behaving as pipe-like conduits that concentrate high-flux flow.

The presence of incrementally deposited orogenic Au–quartz lodes hosted in compressional–transpressional fault structures exhumed from depths comparable to the base of the crustal seismogenic zone provides evidence for localized invasion of large volumes of overpressured H_2O–CO_2 fluids. Only rarely do the vein systems extend for more than a kilometre or so along-strike or down-dip. On a far greater scale ($L \sim 100$ km) crustal seismicity in areas of active compressional–transpressional tectonics has been shown to correlate with areas of reduced *Vs*, while nucleation sites of larger earthquakes correlate with high *Vp/Vs* anomalies ($L \sim 10$ km), both attributable to varying degrees of fluid overpressuring (Christensen 1989, 1996).

Invasion of overpressured fluids into the roots of upper crustal brittle faults promotes *dual-driven* failure where frictional instability is triggered by a combination of increasing shear stress and rising pore-fluid pressure. At depths in excess of a few kilometres, swarms of hydrothermal extension veins define regions where the tensile overpressure condition ($P_f > \sigma_3$) has been met with pore-fluid pressures at near-lithostatic levels. Extension veins are predominantly subhorizontal in compressional regimes, reflecting lithostatic fluid overpressures. The base of the upper crustal seismogenic zone (b.s.z.) at depths of 10–20 km in compressional regimes then becomes a favoured horizon for the development of near-lithostatically overpressured fluid reservoirs made up of fault–fracture meshes distributed throughout substantial rock volumes.

Rupture propagation leads to *fault-valve* action, promoting upwards fluid discharge along the enhanced permeability of the rupture zone, with relief of shear stress accompanied by an abrupt drop in fluid pressure. The most intense valve action is associated with steep reverse faults that are poorly oriented for reactivation and close to frictional 'lock-up' and is thus principally fluid-driven. In these settings, competition often arises between optimally oriented 'Andersonian' thrust faults dipping at ~ 30° and new-formed in the prevailing stress field, and poorly oriented reverse faults dipping > 45°, whose reactivation requires elevated fluid overpressure.

It appears, therefore, that preparation zones for large earthquake ruptures in compressional–transpressional regimes may be defined by the progressive accumulation of fluid overpressure around the base of the seismogenic zone. The 2016 **M** 7.8 Kaikoura multi-rupture provides a possible example. Monitoring the basal region of the seismogenic zone by seismic tomography and/or electrical sounding potentially may help to assess the *'state of preparedness'* for a large earthquake.

Abbreviation

b.s.z.: Base of seismogenic zone.

Acknowledgements

This paper is dedicated to the memory of David P. Hill (1935–2018) of the US Geological Survey, greatly valued friend and mentor. Thanks also to other colleagues in the research fields of Earthquake Science (Tom Hanks, Bill Ellsworth, Tomomi Okada, Stephen Bannister, Francesca Ghisetti) and Mining Geology (John McMahon Moore, Francois Robert, Howard Poulsen, Stephen Cox, Jorge Skarmeta, Clive Willman) and others for generously sharing ideas, field experience, and stimulating discussions over many years. Special thanks to Professor Yoshihisa Iio (DPRI, University of Kyoto) and Associate Professor Tomomi Okada (RCPEVE, Tohoku University, Sendai) for making it possible for me to spend time in their departments and participate in the 2nd Crustal Dynamics symposium ISCD-2 in Kyoto (March 1–3, 2019).

Authors' contributions

Solo authored. The author read and approved the final manuscript.

Funding

Research leading to this publication was largely self-funded as part of an ongoing retirement project. Travel funds allowing the author to attend the 2nd Crustal Dynamics symposium ISCD-2 in Kyoto (March 1–3, 2019) and visit their departments were kindly made available by Professors Yoshihisa Iio (DPRI, Kyoto University) and Tomomi Okada (RCPEVE, Tohoku University, Sendai).

Availability of data and materials

All datasets employed are contained in the listed references.

Competing interests

I declare no competing interests. However, a manuscript currently in press with SSA Bulletin titled "Dual-Driven Fault Failure in the Lower Seismogenic Zone" has a degree of overlap, focusing on the geological and geophysical evidence for overpressured fluids in the lower seismogenic zone.

Author details

[1] Department of Geology, University of Otago, P.O. Box 56, Dunedin 9054, New Zealand. [2] 60 Brabant Drive, Mapua 7005, New Zealand.

Received: 25 August 2019 Accepted: 18 February 2020
Published online: 04 March 2020

References

Ague JJ, Park J, Rye DM (1998) Regional metamorphic dehydration and seismic hazard. Geophys Res Lett 25:4221–4224

Anderson EM (1905) The dynamics of faulting. Trans Edin Geol Soc 8:387–402

Arora BR, Bansal BK, Prajapati SK, Sutar AK, Nayak S (2017) Seismotectonics and seismogenesis of M_w7.8 Gorkha earthquake and its aftershocks. J Asian Earth Sci 133:2–11

Ash CH (2001) Relationships between ophiolites and gold-quartz veins in the North American Cordillera. Brit Col Geol Surv Bull 108:99–110

Bakun WH, Lindh AG (1985) The Parkfield, California, earthquake prediction experiment. Science 229:61–624

Becker JA, Craw D, Horton T, Chamberlain CP (2000) Gold mineralization near the Main Divide, upper Wilberforce valley, Southern Alps, New Zealand. NZ J Geol Geophys 43:199–215

Bierlein FP, Northover HJ, Groves DI, Goldfarb RJ, Marsh EE (2008) Controls on mineralisation in the Sierra Foothills gold province, central California, USA: a GIS-based reconnaissance prospectivity analysis. Aust J Earth Sci 55:61–78

Bishop DG (1994) Stratigraphic, structural, and metamorphic relationships in the Dansey Pass area, Otago, New Zealand. NZ J Geol Geophys 17:301–335

Böhlke JK (1999) Mother Lode gold. In: Moores EM, Sloan D, Stout DL (eds) Classic cordilleran concepts: a view from California. Boulder, Geol Soc Am Spec Pap, pp 55–67

Bonini M (2007) Interrelations of mud volcanism, fluid venting, and thrust-anticline folding: examples from the external northern Apennines (Emilia-Romagna, Italy). J Geophys Res 112:B08413. https://doi.org/10.1029/2006JB004859
Bonini L, Toscani G, Seno S (2016) Comment on "The May 20 (Mw 6.0 and 29 (Mw 6.0), 2012, Emilia (Po Plain, Northern Italy) earthquakes: new seismotectonic implications from subsurface geology and high-quality hypocenter location" by Carannante et al., 2015. Tectonophysics 688:182–188
Boullier A-M, Robert F (1992) Paleoseismic events recorded in Archean gold-quartz vein networks, Val d'Or, Abitibi, Quebec, Canada. J Struct Geol 14:161–179
Brace WF, Paulding BW, Scholz CH (1966) Dilatancy in the fracture of crystalline rocks. J Geophys Res 71:3939–3953
Briggs R, Troxell B (1955) Effect of Arvin-Tehachapi earthquake on spring and stream flow. Cal Div Mines Bull 171:81–98
Byerlee JD (1978) Friction of rocks. Pure Appl Geophys 116:615–626
Carmichael DM (1991) Metamorphism, metasomatism, and Archean lode gold deposits. In: Robert F, Sheahan PA, Green SB (eds) Greenstone Gold and Crustal Evolution. Proc. Geol. Assoc. Canada NUNA Conference, Val d'Or, Quebec, Canada, 142–143
Castillo DA, Zoback MD (1995) Systematic stress variations in the southern San Joaquin Valley and along the White Wolf fault: Implications for the rupture mechanics of the 1952 $\boldsymbol{M}_s$ 7.8 Kern County earthquake and contemporary seismicity. J Geophys Res 100(B4):6249–6264
Célérier B (2008) Seeking Anderson's faulting in seismicity: a centennial celebration. Rev Geophys 46:RG4001. https://doi.org/10.1029/2007RG000240
Christensen NI (1989) Pore pressure, seismic velocities, and crustal structure. In: Pakiser LC, Mooney WD, eds. Geophysical Framework of the Continental United States. Geol Soc Am Mem 172:783–798
Christensen NI (1996) Poisson's ratio and crustal seismology. J Geophys Res 101:3139–3156
Colletinni C, Sibson RH (2001) Normal faults, normal friction. Geology 29:927–930
Cox SF (1995) Faulting processes at high fluid pressures: an example of fault-valve behavior from the Wattle Gully Fault, Victoria, Australia. J Geophys Res 100:12841–12859
Cox SF (2016) Injection-driven swarm seismicity and permeability enhancement: implications for the dynamics of hydrothermal ore systems in high fluid-flux, overpressured faulting regimes—an invited paper. Econ Geol 111:559–587
Cox SF, Wall VJ, Etheridge MA, Potter TF (1991) Deformational and metamorphic processes in the formation of mesothermal, vein-hosted gold deposits—examples from the Lachlan fold-belt in central Victoria, Australia. Ore Geol Rev 6:391–423
De Ronde CEJ, Sibson RH, Bray CJ, Faure K (2001) Fluid chemistry of veining associated with an ancient microearthquake swarm, Benmore Dam, New Zealand. Geol Soc Am Bull 113:1010–1024
Eberhart-Phillips D (1989) Active faulting and deformation of the Coalinga Anticline as interpreted from three-dimensional velocity structure and seismicity. J Geophys Res 94(15):565–586
Eberhart-Phillips D, Bannister S (2010) 3-D imaging of Marlborough, New Zealand, subducted plate and strike-slip fault systems. Geophys J Int 182:73–96
Eberhart-Phillips D, Stanley WD, Rodriguez BD, Lutter WJ (1995) Surface seismic and electrical methods to detect fluids related to faulting. J Geophys Res 100:919–936
Ellsworth WL (2013) Injection-induced earthquakes. Science. https://doi.org/10.1126/science.1225942
Ellsworth WL, Giardini D, Townend J, Ge S, Shimamoto T (2019) Triggering of the Pohang, Korea, earthquake ($\boldsymbol{M}_w$ 5.5) by enhanced geothermal system stimulation. Seismol Res Lett 90:1844–1858
England PC, Thompson AB (1984) Pressure-Temperature-Time paths of regional metamorphism I. Heat transfer during the evolution of regions of thickened continental crust. J Petrol 25:894–928
Etheridge MA (1983) Differential stress magnitudes during regional deformation and metamorphism: upper bound imposed by tensile fracturing. Geology 11:231–234
Etheridge MA, Wall VJ, Cox SF, Vernon RH (1984) High fluid pressures during regional metamorphism and deformation: implications for mass transport and deformation mechanisms. J Geophys Res 89:4344–4358
Foxford KA, Nicholson R, Polya DA, Hebblethwaite RPB (2000) Extensional failure and hydraulic valving at Minas da Panasqueira, Portugal: evidence from vein spatial distributions, displacements and geometries. J Struct Geol 22:1065–1086
Fraser-Smith AC, Bernardi A, Helliwell RA, McGill PR, Villard OG, (1995) Analysis of low-frequency electromagnetic field measurements near the epicenter. US Geol Surv Prof Pap 1550-C:C17–C25
Fyfe WS, Price NJ, Thompson AB (1978) Fluids in the Earth's Crust. Elsevier, Amsterdam, p 381
Galis M, Ampuero JP, Mai PM, Cappa F (2017) Induced seismicity provides insight into why earthquake ruptures stop. Sci Adv 3:7528
Graham CM, England PC (1976) Thermal regimes and regional metamorphism in the vicinity of overthrust faults: an example of shear heating and inverted metamorphic zonation from Southern California. Earth Planet Sci Lett 31:142–152
Grigoli F, Cesca S, Rinaldi AP, Manconi A, Lopez-Comino JA, Clinton JF, Westaway R, Cauzzi C, Daham T, Wiemer S (2018) The November 2017 M_w 5.5 Pohang earthquake: a possible case of induced seismicity in South Korea. Science 360:1003–1006
Groves DI, Goldfarb RJ, Gebre-Mariam M, Hagemann SG, Robert F (1998) Orogenic gold deposits: a proposed classification in the context of their crust distribution and relationship to other gold deposit types. Ore Geol Rev 13:7–27
Groves DI, Santosh M, Goldfarb RJ, Zhang L (2018) Structural geometry of orogenic gold deposits: implications for exploration of world-class and giant deposits. Geosci Front 9:1163–1177
Guj P, Fallon M, McCuaig TC, Fagan R (2011) A time series audit of Zipf's Law as a measure of terrane endowment and maturity in mineral exploration. Econ Geol 106:241–259
Hacker B (1997) Diagenesis and fault valve seismicity of crustal faults. J Geophys Res 102(24):459–467
Hamling IJ, Hreinsdóttir S, Clark K, Elliot J, Liang C, Fielding E, Litchfield N, Villamor P, Wallace L, Wright TJ, D'Anastasio E, Bannister S, Burbidge D, Deny P, Gentle P, Howarth J, Mueller C, Palmer N, Pearson C, Power W, Barnes P, Barrell DJA, Van Dissen R, Langridge R, Little T, Nicol A, Pettinga J, Rowland J, Stirling M (2017) Complex multifault rupture during the 2016 $\boldsymbol{M}_w$ 7.8 Kaikoura earthquake New Zealand. Science. https://doi.org/10.1126/science.aam7194
Hasegawa A (2017) Role of H_2O in generating subduction zone earthquakes. Monogr Environ Earth Planets 5:1–34
Hasegawa A, Nakajima J, Umino N, Miura S (2005) Deep structure of the northeastern Japan arc and its implications for crustal deformation and shallow seismic activity. Tectonophysics 403:59–75
Henderson IHC, McCaig AM (1996) Fluid pressure and salinity variations in shear-related veins, central Pyrenees, France: implications for the fault-valve model. Tectonophysics 262:321–348
Holl H-G, Barton C (2015) Habanero field—structure and state of stress. In: Proc World Geothermal Congress 2015, Melbourne, Australia, 19–25 April 2015
Hori S, Umono N, Kono T, Hasegawa A (2004) Distinct S-wave reflectors (bright spots) extensively distributed in the crust and upper mantle beneath the Northeastern Japan Arc. J Seismol Soc Japan 56:435–466
Hubbert MK, Rubey WW (1959) Role of fluid pressure in overthrust faulting. Geol Soc Am Bull 70:115–206
Huston DL (1998) The hydrothermal environment. AGSO J Austr Geol Geophys 17:15–30
Ichihara H, Uyeshima M, Sakanaka S, Ogawa T, Mishina M, Ogawa Y, Nishitani T, Yamaya Y, Watanabe A, Morita Y, Yoshimura R, Usui Y (2011) A fault zone conductor beneath a compressional inversion zone, northeastern Honshu, Japan. Geophys Res Lett 38:L09301. https://doi.org/10.1029/2011GL047382
Ichihara H, Mogi T, Tanimoto K, Yamaya Y, Hashimoto T, Uyeshima M, Ogawa Y (2016) Crustal structure and fluid distribution beneath the southern part of the Hidaka collision zone revealed by 3-D electrical resistivity modeling. Geochem Geophys Geosyst 17:1480–1491
Ito K (1999) Seismogenic layer, reflective lower crust, surface heat flow and large inland earthquakes. Tectonophysics 306:423–433

Japas MS, Urbina NE, Sruoga P, Garro JM, Ibañes O (2016) A transient fault-valve mechanism operating in upper crustal level, Sierra Pampeanas, Argentina. J Geodyn 111:142–154
Kayal JR, Zhao D, Mishra OP, De R, Singh OP (2002) The 2001 Bhuj earthquake: tomographic evidence for fluids at the hypocenter and its implications for rupture nucleation. Geophys Res Lett 29:2152. https://doi.org/10.1029/2002GL015177
Kita S, Hasegawa A, Nakajima J, Okada T, Matsuzawa T, Katsumata K (2012) High-resolution seismic velocity structure beneath the Hokkaido corner, northern Japan: arc-arc collision and origins of the 1970 M 6.7 Hidaka and 1982 M 7.1 Urakawa-oki earthquakes. J Geophys Res 117:12301. https://doi.org/10.1029/2012jb009356
Knopf A (1929) The Mother Lode System of California. US Geol Surv Prof Pap. 157
Litchfield NJ, Villamor P, Van Dissen RJ, Nicol A, Barnes PM, Barrell DJA, Pettinga J, Langridge RM, Little TA, Mountjoy JJ, Ries WF, Rowland J, Fenton C, Stirling MW, Kearse J, Berryman KR, Cochran UA, Clark KJ, Hemphill-Haley M, Khajavi N, Jones KE, Archibald G, Upton P, Asher C, Benson A, Cox SC, Gasston C, Hale D, Hall B, Hatem AE, Heron DW, Howarth J, Kane TJ, Lamarche G, Lawson S, Lukovic B, McColl ST, Madugo C, Manousakis J, Noble D, Pedley K, Sauer K, Stahl T, Strong DT, Townsend DB, Toy V, Williams J, Woelz S, Zinke R (2018) Surface rupture of multiple crustal faults in the 2016 M_w 7.8 Kaikoura, New Zealand, earthquake. Bull Seismol Soc Am 108:1496–1520
Lockner DA (1995) Rock failure. In: Ahrens TJ (ed) Rock Physics and Phase Relationships: A Handbook of Physical Constants, AGU Reference Shelf 3:127-147
Loucks RR, Mavrogenes JA (1999) Gold solubility in supercritical hydrothermal brines measured in synthetic fluid inclusions. Science 284:2159–2163
MacPherson BJ, Garven G (1999) Hydrodynamics and overpressure mechanisms in the Sacramento Basin, California. Am J Sci 299:429–466
Marchesini B, Garofalo PS, Menegon L, Mattila J, Viola G (2019) Fluid-mediated, brittle-ductile deformation at seismogenic depth—Part 1: fluid record and deformation history of fault veins in a nuclear waste repository (Olkiluoto Island, Finland). Solid Earth 10:809–838
Matsumoto S, Iio Y, Uehira K, Shibutani T (2005) Imaging of *S*-wave reflectors in and around the hypocentral area of the 2004 mid-Niigata Prefecture earthquake (M6.8). Earth Planets Space 57:557–561
Miller JM, Wilson CL (2004) Structural analysis of faults related to a heterogeneous stress history: reconstruction of a dismembered gold deposit, Stawell, western Lachlan Fold Belt, Australia. J Struct Geol 26:1231–1256
Miller SA, Collettini C, Chiaraluce L, Cocco M, Barchi M, Kaus B (2004) Aftershocks driven by a high-pressure CO_2 source at depth. Nature 427:724–727
Morrow CA, Moore DE, Lockner DA (2001) Permeability reduction in granite under hydrothermal conditions. J Geophys Res 106(B12):30551–30560
Mortimer N (1993) Geological Map of the Otago Schist and adjacent rocks, scale 1:500,000. Inst Geol Nucl Sci, Lower Hutt Geol Map, p 7
Mortimer N (2003) A provisional structural thickness map of the Otago Schist, New Zealand. Am J Sci 303:603–621
Nicholson C, Wesson RL (1990) Earthquake hazard associated with deep well injection—a report to the U.S. Environmental Protection Agency. US Geol Surv Bull 1951, 74 p
Okada T, Umino N, Hasegawa A (2010) Deep structure of Ou mountain range strain concentration zone and the focal area of the 2008 Iwate-Miyagi-Nairiku earthquake, NE Japan—seismogenesis related with magma and crustal fluid. Earth Planets Space 62:347–352
Okada T, Umino N, Hasegawa A, Group for the aftershock observations of the Iwate-Miyagi-Nairiku earthquake in 2008 (2012) Hypocenter distribution and heterogeneous velocity structure in and around the focal area of the 2008 Iwate-Miyagi Nairiku earthquake, NE Japan—possible seismological evidence for a fluid driven compressional inversion earthquake. Earth Planets Space 64:717–728
Osborne MJ, Swarbrick RE (1997) Mechanisms for generating overpressure in sedimentary basins: a reevaluation. Am Assoc Petrol Geol Bull 81:1023–1041
Oxburgh ER (1972) Flake tectonics and continental collision. Nature 239:202–204
Oxburgh ER, England PC (1980) Heat flow and the metamorphic evolution of the Eastern Alps. Eclog Geol Helvet 73:379–398
Parry WT (1998) Fault-fluid compositions from fluid-inclusion observations and solubilities of fracture-sealing minerals. Tectonophysics 290:1–26
Parry WT, Bruhn RL (1990) Fluid-pressure transients on seismogenic normal faults. Tectonophysics 179:335–344
Rabeau O, Royer J-J, Jebrak M, Cheilletz A (2013) Log-uniform distribution of gold deposits along major Archean fault zones. Mineral Deposita 48:817–824
Raleigh CB, Healy J, Bredehoeft J (1976) An experiment in earthquake control at Rangely, Colorado. Science 191:1230–1237
Ramsay JG (1980) The crack-seal mechanism of rock deformation. Nature 284:136–139
Rawat G, Arora BR, Gupta PK (2014) Electrical resistivity cross-section across the Garwhal Himalaya: proxy to fluid-seismicity linkage. Tectonophysics 637:68–79
Robert F, Brown AC (1986) Archean gold-bearing quartz veins at the Sigma Mine, Abitibi greenstone belt, Quebec; Part I. Geologic relations and formation of the vein system. Econ Geol 81:595–616
Robert F, Boullier A-M, Firdaous K (1995) Gold-quartz veins in metamorphic terranes and their bearing on the role of fluids in faulting. J Geophys Res 100(12):861–879
Roeloffs E (1995) A reported streamflow increase. US Geol Surv Prof Pap 1550-C: C47–C51
Ryberg T, Fuis GS (1998) The San Gabriel Mountains bright reflective zone: possible evidence for young mid-crustal thrust faulting in southern California. Tectonophysics 286:31–36
Sato H, Amano K (1991) Relationship between tectonics, volcanism, sedimentation and basin development, Late Cenozoic, central part of Northern Honshu, Japan. Sediment Geol 74:323–343
Secor DT (1965) Role of fluid pressure in jointing. Am J Sci 263:633–646
Sibson RH (1981) Fluid flow accompanying faulting: field evidence and models. In: Simpson DW, Richards, PG, eds. Earthquake Prediction: an International Review AGU Maurice Ewing Series. 4:593–603
Sibson RH (1984) Roughness at the base of the seismogenic zone: contributing factors. J Geophys Res 89:5791–5799
Sibson RH (1985) A note on fault reactivation. J Struct Geol 7:751–754
Sibson RH (1990) Conditions for fault-valve behavior. In: Knipe RJ, Rutter EH (eds) Deformation mechanisms, rheology and tectonics. Geol Soc Lond Spec Publ, London, pp 15–28
Sibson RH (1992) Implications of fault-valve behavior for rupture nucleation and recurrence. Tectonophysics 211:283–293
Sibson RH (1993) Load-strengthening versus load-weakening faulting. J Struct Geol 15:123–128
Sibson RH (1996) Structural permeability of fluid-driven fault-fracture meshes. J Struct Geol 18:1031–1042
Sibson RH (2000) A brittle failure mode plot defining conditions for high flux flow. Econ Geol 95:41–47
Sibson RH (2003) Brittle failure controls on maximum sustainable over pressure in different tectonic regimes. Am Assoc Petrol Geol Bull 87:901–908
Sibson RH (2007) An episode of fault-valve behavior during compressional inversion—The 2004 M_J6.8 Mid-Niigata Prefecture, Japan, earthquake sequence. Earth Planet Sci Lett 257:188–199
Sibson RH (2009) Rupturing in overpressured crust during compressional inversion—the case from NE Honshu, Japan. Tectonophysics 473:404–416
Sibson RH (2012) Reverse fault rupturing: competition between non-optimal and optimal fault orientations. In: Healy D, Butler RWH, Shipton ZK, Sibson RH (eds) Faulting, Fracturing, and Igneous Intrusion in the Earth's Crust. Geol Soc Lond Spec Publ, Boulder, pp 39–50
Sibson RH (2014) Earthquake rupturing in fluid-overpressured crust: how common? Pure & Appl Geophys 171:2867–2885
Sibson RH (2017) Tensile overpressure compartments on low-angle thrust faults. Earth Planets Space 69:1–15
Sibson RH (2020) Dual-driven fault failure in the lower seismogenic zone. Bull Seismol Soc Am 1:1–13. https://doi.org/10.1785/0120190190
Sibson RH, Ghisetti FC (2018) Factors affecting the assessment of earthquake hazard from compressional inversion structures. Seismol Soc Am Bull 1088:1819–1836
Sibson RH, Scott J (1998) Stress/fault controls on the containment and release of overpressured fluids: examples from gold-quartz vein system in

Juneau, Alaska, Victoria, Australia and Otago, New Zealand. Ore Geol Rev 13:293–306
Sibson RH, Xie G (1998) Dip range for intracontinental reverse fault ruptures: truth not stranger than friction? Seismol Soc Am Bull 88:1014–1022
Sibson RH, Robert F, Poulsen KH (1988) High-angle reverse faults, fluid-pressure cycling, and mesothermal gold-quartz deposits. Geology 16:551–555
Sieh K (1996) The repetition of large earthquake ruptures. Proc Nat Acad Sci USA 93:3764–3771
Silvio S, Tenthorey E, Cox S, Fitzgerald J (2007) Permeability evolution in quartz fault gouge under hydrothermal conditions. J Geophys Res 112:B07202. https://doi.org/10.1029/2006JB004828
Simmons SF, Brown KL (2006) Gold in magmatic hydrothermal solutions and the rapid formation of a giant ore deposit. Science 314:288–291
Simpson G (2001) Influence of compression-induced fluid pressures on rock strength in the brittle crust. J Geophys Res 106(19):465–478
Spörli KB, Anderson HJ (1980) Paleostress axes from mineral striations in faulted Mesozoic basement, Auckland, New Zealand. NZ J Geol Geophys 23:155–166
Spudich P (1996) Synopsis—main-shock characteristics. US Geol Surv Prof Pap 1550-A:A1–A7
Takei Y (2002) Effect of pore geometry on Vp/Vs: from equilibrium geometry to crack. J Geophys Res. https://doi.org/10.1029/2001JB000522
Tikoff B, Greene D (1997) Stretching lineations in transpressional shear zones. J Struct Geol 19:29–39
Townend J, Zoback MD (2000) How faulting keeps the crust strong. Geology 28:399–402
Tunks AJ, Selley D, Rogers JR, Brabham G (2004) Vein mineralization at Damang Gold Mine, Ghana: controls on mineralization. J Struct Geol 26:1257–1273
Turner J, Williams G (2004) Sedimentary basin inversion and intra-plate shortening. Earth Sci Rev 65:277–304
Wang Z, Zhao D (2006) Seismic images of the source area of the 2004 Mid-Niigata prefecture earthquake in Northeast Japan. Earth Planet Inter 244:16–31
Wang H, Zhao D, Huang Z, Xu M, Wang L, Nishizono Y, Inakura H (2018) Crustal tomography of the 2016 Kumamoto earthquake area in West Japan using *P* and *PmP* data. Geophys J Int 214:1151–1163
Wilkinson JJ, Johnston JD (1996) Pressure fluctuations, phase separation, and gold precipitation during seismic fracture propagation. Geology 24:395–398
Willemse EJM, Pollard DD (1998) On the orientation and patterns of wing cracks and solution surfaces at the tips of a sliding flaw or fault. J Geophys Res 103:2427–2438
Willman CE (2007) Regional structural controls of gold mineralization, Bendigo and Castlemaine goldfields, Central Victoria, Australia. Mineral Deposita 42:449–463
Yerkes RF, Levine P, Wentworth CM (1990) Abnormally high fluid pressures in the region of the Coalinga earthquake sequence and their significance. US Geol Surv Prof Pap 1487:235–257
Zhao D, Negishi H (1998) The 1995 Kobe earthquake: seismic image of the source zone and its implications for the rupture nucleation. J Geophys Res 103:9967–9986
Zhao D, Tani H, Mishra OP (2004) Crustal heterogeneity in the 2000 Western Tottori earthquake region: effects of fluids from slab dehydration. Phys Earth Planet Int 145:161–177
Zoback M-L (1992) First- and second-order patterns of stress in the lithosphere: the World Stress Map Project. J Geophys Res 97(B8):11703–11728
Zoback MD, Beroza GC (1993) Evidence for near-frictionless faulting in the 1989 (M 6.9) Loma Prieta, California, earthquake and its aftershocks. Geology 21:181–185

Publisher's Note